nature water

Supplementary information

https://doi.org/10.1038/s44221-025-00522-8

Hydroclimate and landscape diversity drive highly variable greenhouse gas emissions from tropical and subtropical inland waters

In the format provided by the authors and unedited

Table of contents

Discussion S1. Flux estimation methods

We included both direct (floating chambers, eddy covariance or tracer gas) and indirect (using empirical gas exchange models) flux estimates from the literature. This approach is consistent with our workflow, which involves estimating fluxes at sites where only concentration data are available – we reasoned that indirect flux calculations are likely more accurate when conducted by the original authors, who had access to site-specific information (such as wind speed or discharge), than by applying a coarser approach ourselves. Approximately 28% of riverine flux values and 64% of lake flux values were from direct measurements, while 72% and 36% were derived indirectly (Table S1). The lower proportion of direct flux measurements in streams and rivers is not surprising given the challenges of measuring gas emissions in these systems[1,2].

Table S1. Proportion of direct and indirect flux estimates across climate classes for the river and lake datasets prior to averaging per site. "Direct" refers to in-situ measurements using floating chambers, eddy covariance or tracer gas techniques, while "Indirect" refers to fluxes estimated from gas concentrations combined with gas exchange models or from mass balance calculations. Further details on individual methods are provided in Table S2.

		TOTAL	humid	wet-dry	arid	humid sub.	highland
rivers	Direct	28%	33%	27%	46%	25%	54%
	Indirect	72%	67%	73%	54%	75%	46%
lakes	Direct	64%	97%	73%	93%	58%	36%
	Indirect	36%	3%	27%	7%	42%	64%

A closer look at the distribution of methods across GHGs shows that most direct flux estimates were obtained via floating chambers, while most indirect estimates were obtained using empirical models (Table S2). The highest propotion of direct estimates was for CH_4 diffusion fluxes in lakes (76%), while direct N_2O fluxes only represented 4% of estimates in rivers and 40% in lakes.

We then assessed the differences in flux estimates between methods. We found significant yet non-systematic differences between direct and indirect flux measurements (Tables S3 and S4), with direct methods yielding estimates that were sometimes higher and sometimes lower than those based on indirect methods. Rather, variations across climate classes were greater than any variation attributable to method alone. This suggests that observed spatial patterns are unlikely to be driven by methodological differences. In addition, it is well recognised that chambers will not capture the very high fluxes common in turbulent headwater streams[2], while in slow-flowing streams anchored chambers tend to overestimate fluxes[1] – hence for rivers an exact agreement between methods should not be expected.

Table S2. Number of flux measurements across methods and gases for the river and lake datasets prior to averaging per site site (i.e. n=number of observations). $F_{CH4\ diff}$ and $F_{CH4\ eb}$ refer to the diffusive and ebullitive components of the CH_4 flux, respectively.

		F_{CO2}	F_{CH4} diff	F_{CH4} eb	F_{N2O}
rivers	direct - floating chamber	1739 (26%)	1086 (29%)	129 (86%)	51 (7%)
	direct - bubble trap	-	-	21 (14%)	-
	direct - tracer gas	51 (1%)	-	-	-
	indirect - gas exchange model	4253 (65%)	2625 (71%)	-	654 (93%)
	indirect - mass balance	524 (8%)	-	-	-
	TOTAL	6567	3711	150	705
lakes	direct - floating chamber	1285 (50%)	1757 (76%)	214 (79%)	91 (40%)
	direct - bubble trap	-	-	32 (12%)	-
	direct - eddy covariance	24 (1%)	2 (0%)	-	-
	direct - echosounder	-	-	21 (8%)	-
	indirect - gas exchange model	1205 (47%)	551 (24%)	-	108 (48%)
	indirect - other	60 (2%)	-	-	26 (12%)
	TOTAL	2574	2310	286	225

Table S3. Comparison (non-paired) of median (interquartile interval; n=number of observations) riverine fluxes (mmol/m^2/d) of CO_2, CH_4 (diffusive) and N_2O between direct and indirect methods. These values are derived from independent datasets, not matched site-by-site measurements. The p-values were obtained using Wilcoxon rank-sum tests, with significant differences ($p<0.01$) noted in bold. Definitions of direct and indirect methods are provided in the caption of Table S1. Please note these are unpaired comparisons and do not provide a methodological evaluation of indirect versus direct flux estimates.

		CO_2	CH_4	N_2O
TOTAL	Direct	189.4 (64.8–535.7; n=1790)	0.937 (0.277–4.476; n=1086)	0.018 (0.011–0.043; n=51)
	Indirect	193.1 (63.8–516.2; n=4777)	0.527 (0.138–1.804; n=2625)	0.005 (0.000–0.041; n=654)
	p-value	0.710	**<0.01**	**<0.01**
humid	Direct	361.0 (129.6–889.9; n=408)	0.671 (0.260–1.858; n=272)	0.043 (0.014–0.226; n=19)
	Indirect	195.7 (113.0–522.7; n=675)	0.927 (0.284–2.947; n=419)	0.013 (0.002–0.079; n=360)
	p-value	**<0.01**	0.115	**<0.01**
wet-dry	Direct	250.6 (94.9–595.1; n=329)	0.799 (0.277–1.800; n=142)	0.013 (0.008–0.017; n=2)
	Indirect	102.2 (56.6–442.8; n=1108)	1.161 (0.456–4.219; n=132)	0.012 (-0.002–0.033; n=79)
	p-value	**<0.01**	**<0.01**	-
arid	Direct	67.2 (21.8–123.6; n=39)	1.057 (0.433–1.832; n=15)	n=0
	Indirect	172.0 (84.8–390.2; n=37)	1.195 (0.309–8.710; n=21)	0.125 (0.033–0.584; n=5)
	p-value	**<0.01**	0.974	-
humid sub.	Direct	139.6 (43.7–361.5; n=888)	1.406 (0.310–15.012; n=623)	0.013 (0.009–0.033; n=24)
	Indirect	261.8 (59.9–523.7; n=2835)	0.448 (0.111–1.489; n=2024)	0.001 (0.000–0.002; n=208)
	p-value	**<0.01**	**<0.01**	**<0.01**
highland	Direct	143.8 (52.3–3106.6; n=116)	0.221 (0.104–1.249; n=32)	0.018 (0.012–0.021; n=3)
	Indirect	201.1 (105.0–419.2; n=118)	0.597 (0.136–1.708; n=29)	0.002 (0.002–0.003; n=2)
	p-value	0.875	0.382	-

Table S4. Comparison (non-paired) of median (interquartile interval; n=number of observations) lake fluxes (mmol/m^2/d) of CO_2, CH_4 (diffusive) and N_2O between direct and indirect methods. These values are derived from independent datasets, not matched site-by-site measurements. The p-values were obtained using Wilcoxon rank-sum tests, with significant differences ($p<0.01$) noted in bold. Definitions of direct and indirect methods are provided in the caption of Table S1.

		CO_2	**CH_4**	**N_2O**
TOTAL	Direct	30.2 (-0.1–135.4; n=1309)	0.430 (0.136–1.518; n=1761)	0.010 (0.000–0.030; n=91)
	Indirect	19.1 (0.6–67.3; n=1265)	0.101 (0.021–0.398; n=551)	0.001 (-0.001–0.022; n=134)
	p-value	0.0543	**<0.01**	0.0158
humid	Direct	28.3 (3.9–142.0; n=318)	0.672 (0.341–1.611; n=315)	0.093 (0.002–0.138; n=10)
	Indirect	6.8 (5.1–24.8; n=7)	0.811 (0.198–13.972; n=11)	0.003 (0.000–0.009; n=4)
	p-value	0.195	0.639	0.24
wet-dry	Direct	19.8 (0.2–88.8; n=122)	1.302 (0.314–7.818; n=169)	0.007 (-0.001–0.025; n=56)
	Indirect	0.1 (-4.4–6.1; n=47)	0.106 (0.072–0.481; n=44)	-0.000 (-0.002–0.001; n=39)
	p-value	**<0.01**	**<0.01**	**<0.01**
arid	Direct	113.7 (4.7–249.9; n=6)	3.573 (0.622–13.662; n=14)	n=0
	Indirect	9.0 (6.3–11.7; n=2)	n=0	n=0
	p-value	-	-	-
humid sub.	Direct	34.3 (-5.6–145.7; n=846)	0.310 (0.108–1.203; n=1209)	0.022 (0.007–0.027; n=25)
	Indirect	24.8 (1.9–82.0; n=1058)	0.084 (0.016–0.337; n=459)	0.017 (0.001–0.053; n=75)
	p-value	0.692	**<0.01**	0.627
highland	Direct	2.5 (-9.5–21.3; n=17)	0.481 (0.127–7.706; n=54)	n=0
	Indirect	-1.8 (-24.8–20.6; n=141)	0.073 (0.034–0.372; n=27)	-0.001 (-0.002–-0.001; n=6)
	p-value	0.445	**<0.01**	-

Discussion S2. Data coverage and seasonal variability

Diel variability is an important factor to account for, as higher GHG concentrations and emissions have been reported at night in flowing waters[3,4] while higher fluxes are usually observed during day-time in standing waters[5,6]. In our riverine dataset, around 1% of sites (n=39) have data obtained at a high frequency (i.e. infra-hourly). For these sites, we extracted daily means prior to entering the data into our dataset, so that these daily averages capture the diel variability at these locations. While the proportion of high-frequency measurements in our database is low, a closer examination of the results in Gómez-Gener et al.[3] suggests that the tropical sites in that study tend to have less pronounced day–night CO_2 differences compared to temperate and boreal sites. This seems to be particularly the case in streams where high dissolved organic matter limits light penetration, reducing the variations in CO_2 and O_2 and thus indirectly reducing the diel changes in CH_4 and N_2O as well[7]. As a result, diel patterns may not be as critical for tropical riverine emission estimates, although we acknowledge the uncertainty here as well.

Diel variability is also likely to be less significant in standing water bodies of the tropics relative to temperate systems. In a study of African lakes, diel changes in CO_2 and CH_4 concentrations were found to be modest compared to spatial gradients within lakes and to cross-lake

differences[8]. It was also suggested that differences in emissions rates might arise from diel cycles of wind speed, which are typically higher during day time[8] due to land–lake air temperature gradients. However, we lack studies that contextualise this diel variability in comparison to seasonal differences. Recent work in temperate ponds suggests that seasonal and cross-system differences are much greater than diel variability, and therefore a stronger driver of annual fluxes[9].

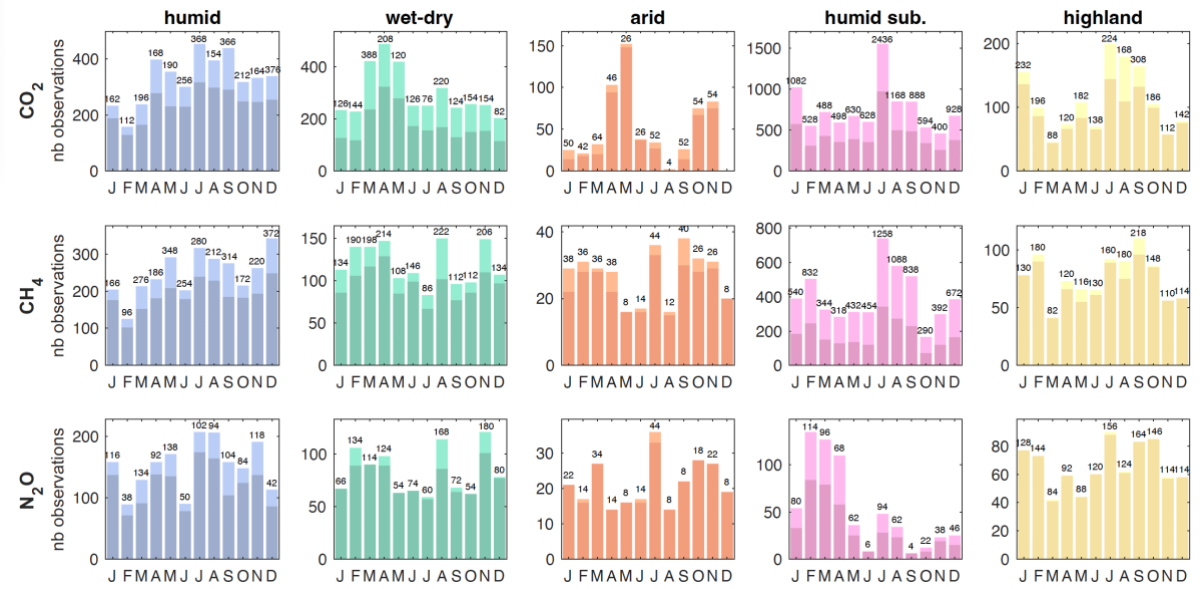

Figure S1a. Monthly distribution of all riverine GHG concentration (darker, lower bars) and flux (lighter, upper bars) measurements available for each climate zone (dataset pre-averaging). The numbers above bars indicate the number of sites with at least one measurement for a given month. CH_4 values represent diffusive emissions only.

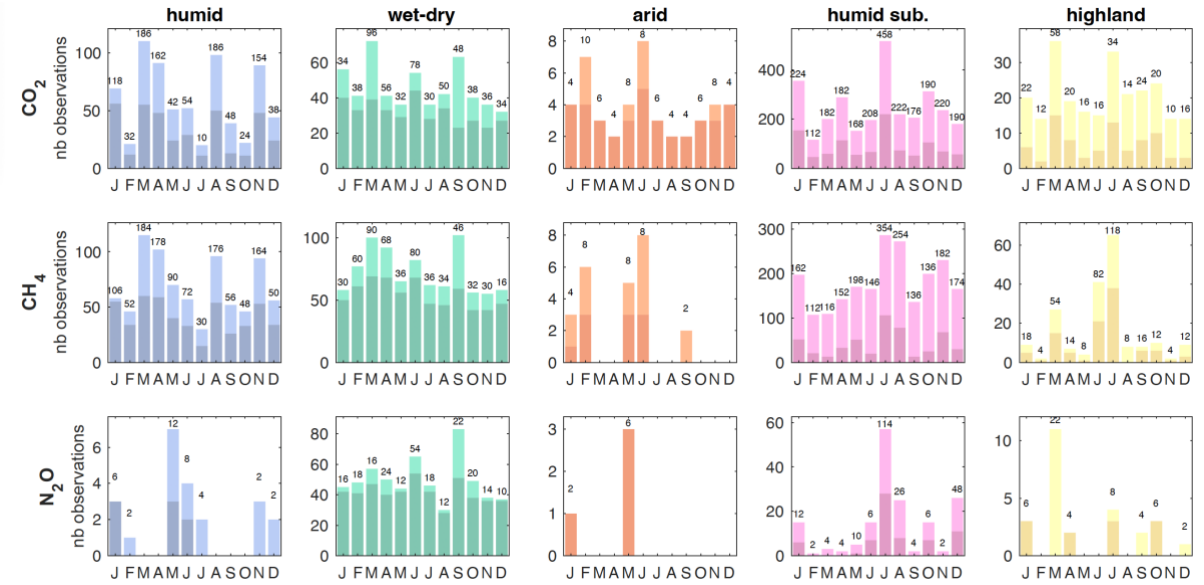

Figure S1b. Monthly distribution of all lake GHG concentration (darker, lower bars) and flux (lighter, upper bars) measurements available for each climate zone (dataset pre-averaging). The numbers above bars indicate the number of systems with at least one measurement for a given month. CH_4 values represent diffusive emissions only.

Integrating seasonal variability is critical to accurate annual flux estimates, and our database does capture some of this variability, with both concentration and flux data relatively evenly distributed throughout the year across all climate zones (Figure S1). Furthermore, examination of the temporal resolution of observations in the database (Table S5) shows that while a significant proportion of sites have one-off measurements (48% for rivers and 43% for lakes), the majority of sites have data collected at a seasonal (or higher) frequency (52% for rivers and 57% for lakes). This is true across all five climate classes, with between 32% (wet-dry tropics) and 83% (arid tropics) of riverine sites having seasonal data, i.e. at least three data points across a given year, and between 6% (humid tropics) and 37% (highland tropics) of riverine sites having a monthly or higher measurement frequency. Similarly, between 28% (highland areas) and 84% (wet-dry tropics) of lake sites have seasonal data, and between 10% (highland areas) and 25% (arid tropics) of lake sites have a monthly or higher measurement frequency. Note that the seasonal variations in lake primary productivity, which is a major driver of GHG emissions, tend to be lower in the tropics than at higher latitudes[10].

Overall, while we acknowledge that the dataset has limitations, we are confident that it captures seasonal variability to a meaningful degree, particularly when compared to previous efforts. The proportion of sites with seasonal or higher temporal resolution across climate zones provides a solid basis for estimating annual fluxes, even if there is still room for improvement in data density and coverage.

Table S5. Measurement frequencies across all sites in the river and lake datasets and within each climate class. Note that the frequency reported in studies and in our database can be lower than the measurement frequency shown here, e.g. for papers that do not provide raw data. Values indicate the number of sites and percentages in parentheses represent the proportion of sites with that frequency within each climate class.

		TOTAL	**humid**	**wet-dry**	**arid**	**humid sub.**	**highland**
rivers	single	1631 (48%)	403 (65%)	343 (68%)	11 (17%)	769 (40%)	105 (39%)
	seasonal	1026 (30%)	176 (29%)	112 (22%)	42 (64%)	631 (33%)	65 (24%)
	monthly	619 (18%)	12 (2%)	27 (5%)	6 (9%)	487 (25%)	87 (33%)
	fortnightly	17 (0.5%)	5 (0.8%)	8 (2%)	2 (3%)	2 (0.1%)	-
	weekly	33 (1%)	10 (2%)	1 (0.2%)	-	15 (0.8%)	7 (3%)
	daily	12 (0.4%)	2 (0.3%)	4 (0.8%)	3 (5%)	3 (0.2%)	-
	high-frequency	39 (1%)	8 (1%)	9 (2%)	2 (3%)	17 (0.9%)	3 (1%)
lakes	single	165 (43%)	5 (16%)	24 (31%)	4 (33%)	84 (43%)	48 (72%)
	seasonal	145 (38%)	21 (66%)	37 (47%)	5 (42%)	69 (35%)	13 (19%)
	monthly	51 (13%)	3 (9%)	13 (17%)	2 (17%)	28 (14%)	5 (8%)
	fortnightly	8 (2%)	-	1 (1%)	-	7 (4%)	-
	weekly	4 (1%)	2 (6%)	1 (1%)	-	1 (1%)	-
	daily	8 (2%)	1 (3%)	1 (1%)	1 (8%)	4 (2%)	1 (2%)
	high-frequency	3 (1%)	-	1 (1%)	-	2 (1%)	-

Discussion S3. Approaches to scaling riverine and lake emissions

Rivers

We adopted a data-driven approach to upscale GHG emissions from flowing waterbodies which, unlike recent modelling studies[11,12], did not explicitly consider seasonal variations in discharge, which drive in part seasonal variations in riverine GHG emissions. However, our dataset does capture these temporal variations as it includes GHG measurements collected throughout the year (Discussion S1; Figure S1), reflecting both high flow and low flow conditions with a similar number of observations. We therefore argue that our flux estimates provide realistic values given they are based on high-volume observations.

Like other large-scale studies, our approach to upscaling riverine fluxes is susceptible to overestimating emissions in low-order streams. This overestimation occurs because upscaling relies on low spatial resolution products, which can artificially combine high GHG concentrations with high gas transfer velocities – conditions that are unlikely to coexist within river networks[13,14]. In small streams, this issue is particularly relevant, as negative relationships between GHG concentration and discharge have been reported[15]. However, in large tropical rivers, the opposite trend is often observed, with CO_2 concentrations increasing with discharge at annual scales[16,17], meaning that high GHG concentrations can coincide with high gas transfer velocities in higher-order rivers. Since our analysis is partly based on direct measurements rather than model outputs, it may be less prone to such potential overestimations in small streams. Nonetheless, process-based models may become a viable alternative in the future to address this issue[18-20]. While these models are showing promise in reducing uncertainties, they will require substantial amounts of new data for calibration and validation.

Lakes

Our approach to scaling lake and reservoir emissions involved binning flux data across all climate zones, because of a scarcity of data for individual climate zones (see Methods). It is possible that this conservative approach resulted in our estimates being biased slightly low as it may have led to (1) an underestimation of CO_2 fluxes in warmer regions such as the humid and wet-dry tropics, (2) an overestimation of N_2O fluxes in systems that are not in the humid subtropics, where fluxes and concentrations tend to be higher (Table S16), and (3) an underestimation of CH_4 fluxes in drier regions such as the (semi)arid tropics. The latter is because CH_4 emissions are enhanced by aquatic primary production[8], which can be higher in lakes under drier climates[10,21] compared to more humid regions where light penetration is lower due to higher dissolved organic matter concentrations[21]. However, our dataset contains many new data from large systems (116 waterbodies > 100 km^2 and 62 waterbodies > 1,000 km^2), whereas previous studies typically had few or no data from these large systems. Given that large waterbodies account for the majority of the (sub)tropical lake area (70% for waterbodies > 100 km^2 and 48% for waterbodies > 1,000 km^2; Table S13), our synthesis should offer a more reliable quantification of their contribution to overall emissions.

Means versus medians

When estimating inland water GHG emissions, the choice between using means or medians influences global upscaling[22]. In our analysis, we used:

(1) means for site-level (rivers) and system-level (lakes/reservoirs) averaging, because means are likely to better capture seasonal variability at individual sites, while medians tend to underestimate the influence of episodic high-flux events. This approach is consistent with previous global meta-analyses[22]. Site-level averaging also avoided biasing results from sites with more frequent sampling.

(2) medians (with interquartile ranges) for the bootstrapping step and reporting of global statistics. This decision was driven by the limited number of observations in many subgroups (i.e. combinations of climate zones and stream orders or lake size classes). In such cases, bootstrapping around means was found to be overly sensitive to extreme values, producing unrealistically high estimates. The use of medians allowed us to reduce the influence of outliers in small subgroups – also consistent with previous work[22].

Regarding (1), our analysis shows that (sub)tropical emission estimates based on site-level averaging by means versus medians are not significantly different for most gases and systems (Table S6), although they differ substantially for diffusive CH_4 fluxes from standing waterbodies, where mean-based estimates are 59% higher (mean difference in bootstrapped area-weighted diffusive flux estimates: 0.13 mmol m^{-2} d^{-1}; 95% confidence interval: 0.03–0.24 mmol m^{-2} d^{-1}). The higher mean-based estimates for diffusive CH_4 likely reflect the episodic nature of these fluxes. Given that at individual sites, means are less likely to underestimate fluxes, we report mean-based estimates (for site-level averaging) in the main text.

Table S6. Upscaled flux estimates (Tg gas/yr) for the global (sub)tropics (median (interquartile range)) based on site-level averaging using medians (left) and means (right).

		Site-level averaging using medians	Site-level averaging using means
lakes	**CO_2**	103.2 (62.0-184.8)	114.4 (73.2-218.6)
	CH_4 diff	0.69 (0.47-1.15)	1.12 (0.62-1.91)
	CH_4 eb	4.36 (1.46-7.21)	4.31 (1.51-7.20)
	N_2O	0.031 (0.021-0.054)	0.032 (0.021-0.052)
rivers	**CO_2**	3,283 (1,944-5,379)	3,387 (2,121-5,702)
	CH_4 diff	4.50 (2.57-7.50)	4.98 (2.80-8.27)
	CH_4 eb	5.16 (0.03-13.86)	5.59 (0.06-15.28)
	N_2O	0.579 (0.329-0.972)	0.615 (0.346-1.102)

Regarding (2), our use of medians instead of means for flux upscaling is a key factor explaining our downward revision of lake CH_4 fluxes. For both diffusive and ebullitive CH_4 fluxes, the previous work by Johnson et al.[23] applied a single mean flux to the entire (sub)tropical lake area (as suggested by the reported means in their Table 2), whereas we used medians for each lake size class. Table S7 provides a direct comparison of median and mean CH_4 fluxes between our dataset and that of Johnson et al.[23]. The study of Johnson et al.[23] used mean diffusive fluxes that are nearly 10 times higher than their median, and mean ebullitive fluxes twice as high as their median. Our dataset is even more skewed, with means more than 50 and 200 times higher

than the medians for diffusive and ebullitive fluxes, respectively – clearly demonstrating that means are influenced by extreme values from small systems at the upper end of the distribution. We believe these highly skewed distributions strongly justify the use of medians for upscaling, as this approach offers a more robust and conservative estimate of typical fluxes, in line with Rosentreter et al.[22].

Table S7. Statistics for the diffusive and ebullitive CH_4 flux observations reported in Johnson et al.[23] (J22) and in our study. For Johnson et al.[23], we included only systems within the (sub)tropical latitude band.

	diffusive CH_4 flux		**ebullitive CH_4 flux**	
	this study	J22	this study	J22
number of systems	327	79	24	23
median (mmol m^{-2} d^{-1})	0.40	0.58	2.01	7.38
mean (mmol m^{-2} d^{-1})	22.21	4.5	467.17	14.67
std (mmol m^{-2} d^{-1})	214.16	10.12	6935.89	27.63

Discussion S4. Remaining uncertainties in flux upscaling

Estimating emissions from inland waters remains a challenging task. Floating chambers (used for flux measurements in 28% and 64% of our river and lake datasets, respectively) can yield biased estimates due to chamber-induced turbulence or sheltering effects[1,24,25]. In turbulent, low-order streams, chambers often underestimate true fluxes due to locally extreme gas exchange rates that cannot be directly measured with a floating chamber[2]. In the absence of direct flux measurements, many riverine studies estimate gas transfer velocity using empirical equations based on hydraulic variables (72% of our river dataset). However, these equations are typically developed for specific flow conditions or stream types[26,27], and can introduce significant uncertainty when applied more broadly. Despite this, we observed relatively good agreement between modelled and measured riverine fluxes in our dataset and residuals were randomly distributed (Figure S2, left panel; R^2=0.73), suggesting that these empirical models provide useful estimates.

For lakes, empirical estimates of gas transfer velocity typically rely on relationships with wind speed (36% of our lake dataset). These relationships are highly variable[28], particularly with regards to lake surface area[24], which plays a key role in determining wind fetch and thus modulates gas transfer velocities[29]. We evaluated three widely used empirical models (VP13[30], CC98[31] and W92[29]; Figure S3b) and retained the two that best matched measured flux data, namely VP13 and CC98. The VP13 model includes a surface area term and was calibrated mainly on small systems (20 lakes ranging from 0.2 to 4 km^2 and one larger reservoir of 600 km^2). It produced higher gas transfer velocity estimates for larger lakes compared to CC98 and W92 (Figure S3a). While this suggest overestimations for large lakes, our VP13-based flux estimates were actually more consistent with measured values, with no apparent size-related bias (Figure S3b). Overall, we found that using the mean of gas transfer velocity estimates from VP13 and CC98 provided flux estimates that aligned relatively well with measured values (Figure S2, right panel; R^2=0.63). The residuals showed no systematic relationship with lake area (not shown), suggesting that model errors were not structured by this variable.

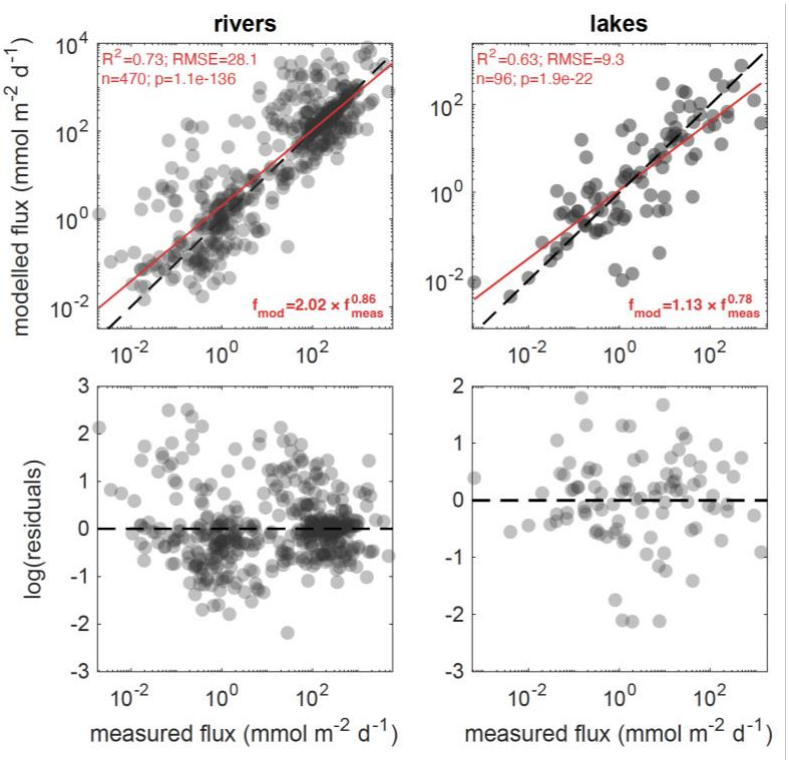

Figure S2. Comparison of measured and modelled GHG fluxes in rivers (left panel) and lakes (right panel). River fluxes were modelled using equation 5 from Raymond et al.[27] while lake fluxes were estimated as the mean of two empirical models[30,31]. Dashed black lines denote the 1:1 relationship; red lines show the fitted power-law regressions.

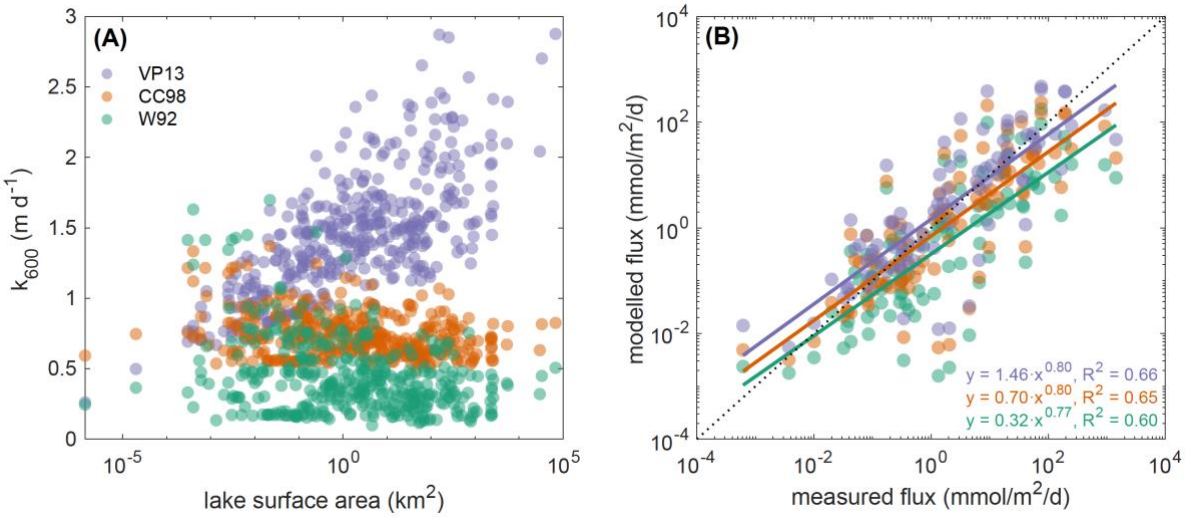

Figure S3. (A) Influence of lake surface area on gas transfer velocity (k_{600}) estimates based on three empirical models[29-31]. (B) Comparison of measured and modelled GHG fluxes in lakes and reservoirs using three empirical models of the gas transfer velocity as a function of wind speed, and using an annual average wind speed from the WorldClim2 database[32]. For sites where only GHG concentrations were reported, we estimated fluxes using the mean of models CC98[31] and VP13[30] as both were closest to the 1:1 line, whereas W92[29] tended to underestimate fluxes, particularly for high flux values.

Our riverine gas transfer velocity estimates were overall lower than those of a previous global study[11], which we attribute to our use of a newer, higher-resolution product for channel slope determination[33]. Our estimates also tended to be lower in first- to third-order streams compared to fourth-order streams (Table S11b). While somewhat unexpected, a similar pattern has been reported for agricultural streams in a large-scale study[34]. In our case, this pattern may partly reflect underestimations of stream slope in low-order streams, potentially due to the limited spatial resolution of the Hydrography90m dataset at these small scales. Lower flow velocities in smaller streams, which are driven by factors such as high streambed roughness[35], likely also play a role. Furthermore, many low-order streams in the humid tropics flow through low-relief landscapes, where the flatter terrain further limits gas transfer velocities[27]. While our GHG fluxes from low-order streams may be slightly underestimated, the magnitude of this effect is uncertain and likely to be modest.

CH_4 ebullition is notoriously difficult to estimate accurately because of its stochastic nature, resulting in intense short-term temporal variability in addition to spatial and seasonal variability. In aquatic systems, CH_4 ebullition can be measured by hydroacoustic methods, eddy-covariance, floating chambers, and stationary bubble traps (inverted funnels), and while these methods have been used extensively in standing waters, their application to flowing waters remains relatively limited. The hydroacoustic method has been used in standing waters[36,37] but is not readily applicable to flowing waters because it requires a minimal depth of 1.5 m. To our knowledge, this technique has only been used in a deep and impounded large European river with physical characteristics resembling standing waters[38]. The application of eddy-covariance in streams and rivers is also very limited[39], while floating chambers have been used in large rivers[40,41] and stationary bubble traps are the most frequently used method in streams[42-50] – although there is a need for methodological standardisation[51]. While the controls on ebullition in rivers are still little understood, river depth and flow velocity have recently been shown to affect ebullition rates negatively[50]. It is therefore possible that ebullition might be higher in smaller streams – although impoundments in large rivers can enhance CH_4 ebullition[52]. Overall, ebullition measurements in flowing waters remain scarce, particularly in the (sub)tropics, and this data gap represents a significant uncertainty in tropical riverine CH_4 budgets.

Surface area estimates of inland waters are another major source of uncertainty. While recent remote sensing efforts such as the Surface Water and Ocean Topography (SWOT) mission have improved our ability to map standing water bodies, challenges remain. Small lakes and ponds, which are potentially important contributors to GHG emissions[53], are still often underrepresented due to resolution limits of present Earth observation sensors. Surface area estimates of smaller water bodies rely on statistical extrapolations[54], which are subject to disputed accuracy[55-58] and carry the risk of double-counting areas with other systems. In our study, we decided to exclude water bodies < 0.01 km^2 due to concerns about accuracy and overlap. While water bodies in this size class have a potentially significant surface area globally[53], these estimates are derived from statistical extrapolation methods that relate lake size to abundance[54]. Such extrapolations may lead to overestimates[55,59] and provide limited ability to control for double-counting with other ecosystems, particularly wetlands. We used lake surface area estimates from the newly released SWOT Prior Lake Database[58] (PLD) for water bodies larger than 0.01 km^2. SWOT PLD showed good agreement for lakes > 0.1 km^2 with estimates from HydroLAKES[60], which is based on national and international inventories

and peer-reviewed datasets. While SWOT PLD is not entirely exempt from overlap with wetland areas, it provides discrete spatial polygons that can allow for comparison against wetland datasets (a task beyond the scope of this study).

Mapping river surface area is equally challenging. This is especially true for low-order streams, which dominate drainage networks but are difficult to detect in satellite imagery due to narrow widths, canopy cover, and high flow intermittency. As a result, global inventories of river surface area tend to underrepresent these smaller streams, despite their potentially important contribution to GHG fluxes[11,12]. To estimate stream surface areas, we used the Global Reach-level A priori Discharge Estimates for SWOT (GRADES) dataset[61]. One limitation of GRADES is that it lacks the spatial resolution needed to capture first-order streams, which introduces significant uncertainty into our area estimates for these small streams. Similar limitations have been reported in recent global studies[11,12]. To help address this issue, we also used the Hydrography90m product[33] for catchment area and stream order classification, which offers a higher spatial resolution and includes more headwater segments. However, we were unable to integrate flow intermittency data to generate realistic surface area estimates with Hydrography90m. Additionally, the low dry-season fraction we estimated for the humid tropics (0.016; Table S8) likely underestimates actual seasonal drying in low-order streams, even in wetter climates. Given these limitations, we applied a broad uncertainty range of ±30% to our surface area estimates. Future efforts that combine high-resolution mapping of low-order streams with network seasonal expansion/contraction will be critical to improve the accuracy of riverine surface area assessments.

Another important gap relates to the role of emergent and submerged vegetation in standing waters. These habitats in the littoral zone of lakes are hotspots of CH_4 production and emission[62-65]. Emergent littoral vegetation also acts as a sink of atmospheric CO_2 that can partly offset the GHG emissions from lakes[66]. While this uptake can represent a substantial flux, we currently lack spatially explicit datasets of littoral vegetation cover, and have little data on carbon and GHG fluxes in vegetated littoral areas. The extent of these zones varies widely across lake types – they are often scarce in saline[67] or phytoplankton-dominated lakes[68], and limited in systems with steep shores such as crater lakes. In large lakes, which we show account for a disproportionate share of total lake surface area and GHG emissions in the tropics (Figure 1; Table S13), the relative cover of vegetated littoral areas is typically low. Additionally, overlap with adjacent wetlands can lead to double counting of fluxes. Taken together, these gaps limit our ability to integrate fluxes from emergent and submerged vegetation at broader scales with an equivalent level of detail and confidence as done here for open-water emissions.

Discussion S5. Role of wetlands in (sub)tropical inland water emissions

The role of tropical riparian wetlands in emitting large quantities of GHG has been highlighted in previous work in the Amazon[69-73] and more recently in the Congo basin[7,74]. Tropical wetland CH_4 emissions account for 53% of global wetland emissions[75], and year-to-year changes in their inundation extent strongly impact the net atmospheric CH_4 growth[76,77]. However, estimates of CH_4 emissions from tropical wetlands are the most uncertain at the global scale[78]. Scaling up wetland measurements remains a challenge due to the difficulty in capturing

seasonal variations in wetland surface area and the high spatial-temporal variability in GHG emissions[79]. We therefore decided not to include these ecosystems in our data compilation. Given the extent of riparian wetlands in the humid tropics[80] and the potential role of (sub)tropical wetland tree stems in emitting CH_4[73,81], and despite substantial loss of global wetland area over the past few centuries[82], it is crucial that future efforts continue reducing uncertainties in the GHG fluxes from these systems. The use of satellite radar interferometry to develop new remote sensing products[80,83] represents a promising approach to more accurate mapping of (sub)tropical wetland extent.

Table S8. River surface areas across stream orders (SO) and climate zones, and weighting factors ('fraction dry') used to account for seasonal variability in river areas. Surface area values are given in km^2, with percentages indicating each value's proportion of the total river surface area.

Climate zone	SO1	SO2	SO3	SO4	SO5	SO6	SO7	SO8	SO9+	fraction dry
humid tropics	46,449 (10.0%)	14,502 (3.1%)	13,176 (2.8%)	15,195 (3.3%)	16,812 (3.6%)	18,918 (4.1%)	12,201 (2.6%)	12,156 (2.6%)	8,158 (1.8%)	0.016
wet-dry tropics	42,956 (9.3%)	11,633 (2.5%)	10,795 (2.3%)	11,193 (2.4%)	13,549 (2.9%)	12,459 (2.7%)	12,326 (2.7%)	11,062 (2.4%)	4,024 (0.9%)	0.162
(semi)arid (sub)tropics	37,857 (8.2%)	9,823 (2.1%)	8,576 (1.9%)	8,121 (1.8%)	7,582 (1.6%)	7,133 (1.5%)	7,838 (1.7%)	4,152 (0.9%)	3,123 (0.7%)	0.422
humid subtropics	19,881 (4.3%)	5,970 (1.3%)	5,642 (1.2%)	6,225 (1.3%)	7,053 (1.5%)	7,551 (1.6%)	5,273 (1.1%)	3,825 (0.8%)	5,160 (1.1%)	0.078
highland (sub)tropics	7,093 (1.5%)	2,094 (0.5%)	1,749 (0.4%)	1,509 (0.3%)	1,268 (0.3%)	1,101 (0.2%)	762 (0.2%)	/	/	0.120

Table S9. Median (interquartile range; n=number of sites) of riverine GHG concentrations across stream orders (SO) and climate zones. Values are expressed in µM (CO_2 and CH_4) and nM (N_2O). For sites with repeated measurements, we calculated a mean value (see Methods).

Climate zone	SO1	SO2	SO3	SO4	SO5	SO6	SO7	SO8	SO9+
CO_2									
humid	289 (103–374; n=39)	254 (113–444; n=21)	199 (80–303; n=17)	132 (75–282; n=12)	182 (78–249; n=32)	53 (42–99; n=40)	94 (65–260; n=54)	78 (51–125; n=28)	92 (68–135; n=140)
wet-dry	225 (120–375; n=38)	129 (59–387; n=19)	78 (63–141; n=31)	75 (52–195; n=29)	79 (45–185; n=42)	89 (53–282; n=54)	79 (56–109; n=65)	64 (42–112; n=30)	101 (53–134; n=75)
arid	42 (41–44; n=2)	69 (17–121; n=2)	1748 (1748–1748; n=1)	60 (48–73; n=2)	69 (41–159; n=6)	47 (28–63; n=10)	41 (31–57; n=16)	49 (40–60; n=7)	59 (33–70; n=15)
humid sub.	163 (64–228; n=75)	104 (58–199; n=64)	80 (44–161; n=148)	65 (41–108; n=238)	71 (43–113; n=302)	94 (54–133; n=216)	91 (64–130; n=165)	97 (57–128; n=88)	73 (53–101; n=95)
highland	89 (54–122; n=39)	75 (45–190; n=24)	68 (41–100; n=37)	49 (35–455; n=41)	91 (40–241; n=42)	100 (36–456; n=34)	50 (39–105; n=13)	31 (9–52; n=2)	52 (35–67; n=4)
CH_4									
humid	0.92 (0.31–3.19; n=89)	1.31 (0.59–5.16; n=28)	0.54 (0.14–2.70; n=23)	0.41 (0.23–1.37; n=30)	0.68 (0.18–1.16; n=48)	0.47 (0.26–1.01; n=32)	0.23 (0.15–0.64; n=89)	0.27 (0.19–0.59; n=26)	0.10 (0.06–0.23; n=131)
wet-dry	0.41 (0.23–2.62; n=26)	0.35 (0.09–1.85; n=19)	0.43 (0.11–1.52; n=38)	0.45 (0.08–1.46; n=39)	0.25 (0.07–0.79; n=43)	0.50 (0.12–1.27; n=49)	0.30 (0.17–0.45; n=49)	0.38 (0.15–0.85; n=22)	0.21 (0.11–0.46; n=64)
arid	3.45 (3.45–3.45; n=1)	0.09 (0.09–0.09; n=1)	0.22 (0.09–0.36; n=2)	0.12 (0.12–0.12; n=1)	0.24 (0.17–0.29; n=4)	0.27 (0.10–0.39; n=5)	0.12 (0.07–0.22; n=14)	0.11 (0.08–0.19; n=7)	0.24 (0.14–0.37; n=14)
humid sub.	0.48 (0.23–1.09; n=122)	0.42 (0.17–1.08; n=78)	0.61 (0.26–1.39; n=161)	0.37 (0.16–1.17; n=161)	0.35 (0.15–0.97; n=162)	0.26 (0.14–0.58; n=97)	0.21 (0.09–0.67; n=46)	0.21 (0.10–0.37; n=31)	0.23 (0.11–0.39; n=75)
highland	0.34 (0.19–0.50; n=29)	0.34 (0.25–1.00; n=22)	0.19 (0.06–0.93; n=37)	0.06 (0.02–0.14; n=37)	0.16 (0.04–0.53; n=33)	0.18 (0.10–0.40; n=25)	0.25 (0.17–0.32; n=8)	0.65 (0.65–0.65; n=1)	0.03 (0.02–0.03; n=4)
N_2O									
humid	8.5 (6.1–13.8; n=17)	7.6 (5.8–10.2; n=15)	12.4 (7.5–13.5; n=9)	9.0 (7.2–12.2; n=22)	7.7 (7.3–11.3; n=22)	7.6 (7.2–8.3; n=20)	8.4 (8.2–9.4; n=8)	7.7 (5.4–15.5; n=14)	8.1 (7.1–9.7; n=25)
wet-dry	11.2 (9.9–38.4; n=18)	8.3 (7.0–11.2; n=14)	8.9 (8.3–12.0; n=23)	8.5 (7.6–10.1; n=23)	7.6 (7.3–8.4; n=18)	8.3 (7.3–10.0; n=27)	8.5 (7.4–9.5; n=39)	8.5 (7.6–9.4; n=18)	7.7 (6.3–9.8; n=28)
arid	65.3 (65.3–65.3; n=1)	n=0	7.6 (7.6–7.6; n=1)	7.1 (7.1–7.1; n=1)	10.1 (8.6–10.9; n=3)	n=0	7.5 (7.3–8.1; n=11)	7.6 (7.0–9.1; n=7)	7.6 (6.9–8.0; n=13)
humid sub.	40.5 (25.3–40.9; n=5)	5.2 (5.0–5.5; n=6)	8.8 (5.0–31.0; n=8)	8.0 (7.1–8.5; n=4)	8.4 (7.2–16.0; n=8)	10.3 (6.7–21.8; n=24)	7.6 (7.1–14.3; n=5)	6.9 (5.8–10.0; n=9)	6.8 (5.8–7.6; n=15)
highland	14.0 (7.9–20.1; n=28)	13.6 (9.7–17.2; n=20)	9.1 (7.9–14.1; n=30)	9.2 (7.7–12.8; n=28)	8.5 (8.0–11.0; n=27)	12.5 (8.5–24.0; n=21)	7.7 (7.0–8.5; n=6)	9.4 (9.4–9.4; n=1)	n=0

Table S10. Median (interquartile range; n=number of sites) of riverine GHG fluxes (mmol m^{-2} d^{-1}) across stream orders (SO) and climate zones. CH_4 fluxes represent diffusive fluxes only. The table includes both measured and modelled fluxes based on measured concentrations (see Methods).

Climate zone	SO1	SO2	SO3	SO4	SO5	SO6	SO7	SO8	SO9+
CO_2									
humid	865 (490–3638; n=40)	924 (460–1491; n=21)	522 (248–1197; n=18)	403 (190–1338; n=12)	490 (153–931; n=35)	154 (102–319; n=41)	306 (162–846; n=56)	163 (130–329; n=32)	264 (176–399; n=154)
wet-dry	1600 (407–5075; n=37)	665 (112–1501; n=19)	246 (74–618; n=37)	251 (93–459; n=35)	185 (79–434; n=47)	244 (133–700; n=60)	250 (97–610; n=67)	169 (97–279; n=32)	238 (121–378; n=75)
arid	177 (79–276; n=2)	4731 (14–9449; n=2)	5103 (5103–5103; n=1)	310 (94–526; n=2)	358 (162–1938; n=6)	304 (131–557; n=10)	90 (42–193; n=16)	187 (89–358; n=7)	107 (36–158; n=15)
humid sub.	501 (174–816; n=100)	247 (88–542; n=84)	284 (85–550; n=174)	298 (147–507; n=258)	226 (110–494; n=333)	270 (118–525; n=255)	195 (93–406; n=199)	184 (98–380; n=91)	118 (52–356; n=111)
highland	633 (210–1472; n=41)	398 (286–1173; n=24)	283 (123–876; n=37)	351 (105–2360; n=44)	467 (97–1074; n=46)	292 (116–5976; n=37)	183 (64–289; n=15)	173 (-67–413; n=2)	156 (67–234; n=4)
CH_4									
humid	8.16 (2.60–23.19; n=90)	11.91 (7.70–30.58; n=28)	5.41 (2.01–26.84; n=23)	7.98 (4.20–12.43; n=31)	5.41 (2.72–12.34; n=49)	5.97 (3.57–9.57; n=32)	1.81 (1.08–4.27; n=89)	3.52 (1.29–13.26; n=31)	1.35 (0.75–3.52; n=141)
wet-dry	12.35 (5.70–95.76; n=26)	7.49 (3.08–28.15; n=20)	6.07 (2.08–21.02; n=38)	6.90 (2.29–22.92; n=42)	4.47 (1.05–8.80; n=43)	4.34 (1.87–21.03; n=52)	4.68 (2.62–9.64; n=49)	3.08 (1.57–7.61; n=23)	1.85 (0.69–4.11; n=64)
arid	67.99 (67.99–67.99; n=1)	0.73 (0.73–0.73; n=1)	1.83 (0.72–2.94; n=2)	0.99 (0.99–0.99; n=1)	10.05 (4.05–14.93; n=4)	2.27 (0.85–3.48; n=5)	1.71 (0.99–3.90; n=14)	1.93 (0.98–2.65; n=7)	1.11 (0.64–4.51; n=14)
humid sub.	2.45 (0.78–7.59; n=130)	2.15 (0.90–5.25; n=93)	2.95 (1.28–9.14; n=175)	2.39 (1.23–10.39; n=164)	2.09 (0.86–5.65; n=166)	1.67 (0.75–5.33; n=113)	1.48 (0.60–4.62; n=68)	1.06 (0.34–1.96; n=31)	1.19 (0.49–2.56; n=78)
highland	7.71 (3.22–17.13; n=29)	10.38 (3.88–14.73; n=22)	10.07 (4.01–21.25; n=37)	3.74 (1.33–9.14; n=40)	3.08 (1.20–6.47; n=34)	4.31 (1.92–12.11; n=25)	5.20 (2.66–10.29; n=8)	18.01 (18.01–18.01; n=1)	0.32 (0.10–0.73; n=4)
N_2O									
humid	0.06 (0.02–0.28; n=28)	0.02 (0.01–0.03; n=15)	0.05 (0.03–0.11; n=9)	0.01 (0.00–0.03; n=23)	0.03 (0.01–0.06; n=22)	0.03 (0.02–0.05; n=20)	0.01 (0.01–0.02; n=8)	0.02 (-0.00–0.07; n=16)	0.02 (0.02–0.03; n=27)
wet-dry	0.34 (0.12–0.73; n=18)	0.31 (0.04–0.74; n=14)	0.06 (0.02–0.28; n=23)	0.22 (0.08–0.66; n=23)	0.07 (0.04–0.11; n=18)	0.03 (0.02–0.05; n=28)	0.05 (0.02–0.12; n=39)	0.02 (0.01–0.05; n=18)	0.01 (-0.00–0.02; n=28)
arid	0.48 (0.48–0.48; n=1)	n=0	0.02 (0.02–0.02; n=1)	0.02 (0.02–0.02; n=1)	0.17 (0.15–0.17; n=3)	n=0	0.03 (0.02–0.07; n=11)	0.04 (0.02–0.06; n=7)	0.01 (0.00–0.01; n=13)
humid sub.	0.02 (0.01–0.05; n=5)	0.00 (0.00–0.00; n=6)	0.05 (0.00–0.11; n=9)	0.04 (0.00–0.19; n=4)	0.11 (0.02–0.17; n=8)	0.04 (0.01–0.24; n=24)	0.02 (0.01–0.10; n=6)	0.00 (0.00–0.02; n=9)	0.00 (-0.00–0.01; n=15)
highland	0.15 (0.05–0.32; n=28)	0.13 (0.10–0.23; n=20)	0.14 (0.07–0.38; n=30)	0.20 (0.10–0.33; n=28)	0.05 (0.04–0.13; n=27)	0.16 (0.05–0.48; n=21)	0.10 (0.08–0.12; n=6)	0.10 (0.10–0.10; n=1)	n=0

Table S11a. Differences between riverine GHG fluxes (mmol m^{-2} d^{-1}) across stream orders (SO). Values are shown as median (interquartile range; n=number of sites). P-values are derived from Kruskal-Wallis tests, and post-hoc groupings based on pairwise Wilcoxon rank-sum tests with Benjamini-Hochberg correction are indicated by letters; stream orders sharing the same letter are not significantly different ($p<0.05$). Flux values include both measured and modelled estimates. P-values <0.05 are shown in bold and those <0.01 are shown in bold and italic.

	CO_2	CH_4	N_2O
***p*-value**	***2.36E-25***	***1.52E-22***	***2.16E-24***
SO1	655 (238–1607; n=220) (a)	1.64 (0.54–6.11; n=276) (a)	0.16 (0.03–0.37; n=80) (a)
SO2	354 (122–835; n=151) (b)	1.54 (0.56–5.36; n=165) (ab)	0.05 (0.01–0.23; n=56) (ab)
SO3	299 (93–605; n=267) (bcd)	1.43 (0.47–5.97; n=275) (ab)	0.08 (0.03–0.27; n=73) (a)
SO4	298 (139–577; n=352) (bc)	1.46 (0.46–4.50; n=278) (ab)	0.11 (0.03–0.30; n=79) (a)
SO5	252 (106–560; n=468) (cd)	1.02 (0.36–2.97; n=296) (c)	0.06 (0.03–0.11; n=78) (b)
SO6	257 (116–592; n=405) (bc)	1.07 (0.34–3.34; n=227) (bc)	0.04 (0.02–0.11; n=93) (b)
SO7	214 (95–475; n=355) (de)	0.72 (0.33–2.14; n=230) (c)	0.03 (0.02–0.09; n=70) (b)
SO8	174 (102–352; n=164) (e)	0.69 (0.34–2.55; n=93) (c)	0.02 (0.00–0.05; n=51) (c)
SO9+	225 (101–381; n=359) (e)	0.44 (0.20–1.16; n=301) (d)	0.01 (0.00–0.02; n=83) (d)

Table S11b. Differences between riverine GHG concentrations and k_{600} estimates (gas transfer velocity at Schmidt number 600) across stream orders (SO). Values are shown as median (interquartile range; n=number of sites). P-values are derived from Kruskal-Wallis tests, and post-hoc groupings based on pairwise Wilcoxon rank-sum tests with Benjamini-Hochberg correction are indicated by letters; stream orders sharing the same letter are not significantly different ($p<0.05$). P-values <0.05 are shown in bold and those <0.01 are shown in bold and italic.

	CO_2 (µM)	CH_4 (µM)	N_2O (nM)	k_{600} (m/d)
***p*-value**	***7.04E-18***	***2.83E-29***	***2.96E-08***	***4.59E-88***
SO1	158 (75–279; n=193) (a)	0.5 (0.2–1.6; n=267) (a)	12.6 (7.9–26.1; n=69) (a)	3.79 (2.17–12.65; n=361) (a)
SO2	107 (59–257; n=131) (a)	0.5 (0.2–1.4; n=149) (a)	8.9 (7.0–13.1; n=56) (bcd)	3.21 (2.08–12.22; n=209) (a)
SO3	81 (45–159; n=234) (b)	0.5 (0.2–1.3; n=261) (a)	9.0 (7.9–13.7; n=72) (ab)	5.61 (2.34–16.52; n=384) (b)
SO4	65 (40–131; n=323) (c)	0.3 (0.1–1.0; n=268) (bc)	8.7 (7.6–12.2; n=78) (bc)	7.40 (3.33–17.64; n=461) (c)
SO5	77 (44–139; n=425) (bc)	0.3 (0.1–0.8; n=290) (bc)	8.2 (7.4–10.7; n=78) (bc)	4.52 (2.73–11.82; n=544) (b)
SO6	87 (50–140; n=356) (b)	0.3 (0.1–0.7; n=208) (b)	8.5 (7.3–14.6; n=92) (bc)	3.53 (2.52–8.21; n=457) (a)
SO7	87 (57–132; n=313) (b)	0.2 (0.1–0.5; n=206) (c)	8.2 (7.3–9.2; n=69) (cd)	2.59 (2.17–5.05; n=443) (d)
SO8	84 (50–126; n=155) (bc)	0.3 (0.1–0.5; n=87) (bc)	8.2 (6.8–9.7; n=49) (cd)	2.55 (2.14–4.52; n=191) (d)
SO9+	85 (55–125; n=329) (b)	0.2 (0.1–0.3; n=288) (d)	7.6 (6.7–9.4; n=81) (d)	2.20 (2.15–2.89; n=418) (e)

Table S12a. Differences between riverine GHG fluxes (mmol m^{-2} d^{-1}) across climate zones. Values are shown as median (interquartile range; n=number of sites). P-values are derived from Kruskal-Wallis tests, and post-hoc groupings based on pairwise Wilcoxon rank-sum tests with Benjamini-Hochberg correction are indicated by letters; climate zones sharing the same letter are not significantly different ($p<0.05$). Flux values include both measured and modelled estimates. P-values <0.05 are shown in bold and those <0.01 are shown in bold and italic.

	CO_2	CH_4	N_2O
***p*-value**	***2.44E-10***	***4.41E-17***	***1.33E-26***
humid	311 (161–600; n=410) (a)	1.25 (0.41–3.96; n=515) (a)	0.02 (0.01–0.05; n=168) (a)
wet-dry	249 (116–655; n=409) (b)	1.62 (0.51–4.56; n=357) (ab)	0.05 (0.02–0.18; n=209) (b)
arid	157 (71–324; n=61) (c)	0.60 (0.29–1.70; n=49) (c)	0.02 (0.01–0.08; n=37) (ab)
humid sub.	249 (103–508; n=1616) (b)	0.71 (0.28–2.20; n=1020) (c)	0.01 (0.00–0.07; n=86) (a)
highland	333 (122–1389; n=250) (a)	1.82 (0.65–5.40; n=200) (b)	0.12 (0.06–0.30; n=161) (c)

Table S12b. Differences between riverine GHG concentrations and k_{600} estimates (gas transfer velocity at Schmidt number 600) across climate zones. Values are shown as median (interquartile range; n=number of sites). P-values are derived from Kruskal-Wallis tests, and post-hoc groupings based on pairwise Wilcoxon rank-sum tests with Benjamini-Hochberg correction are indicated by letters; climate zones sharing the same letter are not significantly different ($p<0.05$). P-values <0.05 are shown in bold and those <0.01 are shown in bold and italic.

	CO_2 (µM)	CH_4 (µM)	N_2O (nM)	k_{600} (m d^{-1})
***p*-value**	***1.32E-15***	***9.73E-11***	***3.60E-09***	***2.08E-78***
humid	101 (64–208; n=384) (a)	0.3 (0.1–1.0; n=497) (a)	8.1 (7.1–11.1; n=152) (a)	2.44 (2.15–3.86; n=647) (a)
wet-dry	92 (56–180; n=383) (a)	0.3 (0.1–0.8; n=349) (a)	8.4 (7.5–10.2; n=208) (a)	3.14 (2.19–8.22; n=503) (b)
arid	48 (33–69; n=61) (b)	0.2 (0.1–0.3; n=49) (b)	7.6 (7.1–8.4; n=37) (a)	3.87 (2.17–9.88; n=65) (bc)
humid sub.	83 (49–133; n=1402) (c)	0.4 (0.2–1.0; n=935) (a)	7.6 (6.2–14.3; n=84) (a)	3.80 (2.34–9.64; n=1990) (c)
highland	72 (40–158; n=236) (c)	0.2 (0.1–0.5; n=196) (b)	10.1 (8.0–15.2; n=161) (b)	12.33 (6.32–33.85; n=267) (d)

Table S13. Surface areas of lakes and reservoirs across size classes and climate zones. Surface area values are given in km^2, with percentages indicating each value's proportion of the total standing water surface area.

Climate zone	0.01-0.1	0.1-1	1-10	10-100	100-1000	>1000
Lakes						
humid tropics	2052 (0.3%)	5071 (0.8%)	8776 (1.4%)	10585 (1.7%)	19215 (3.1%)	76893 (12.5%)
wet-dry tropics	5061 (0.8%)	8181 (1.3%)	9801 (1.6%)	11635 (1.9%)	15203 (2.5%)	105016 (17.1%)
(semi)arid (sub)tropics	2804 (0.5%)	5887 (1.0%)	9452 (1.5%)	16651 (2.7%)	29945 (4.9%)	41774 (6.8%)
humid subtropics	6859 (1.1%)	8138 (1.3%)	7672 (1.2%)	9254 (1.5%)	9740 (1.6%)	13512 (2.2%)
highland (sub)tropics	1202 (0.2%)	1735 (0.3%)	1949 (0.3%)	4720 (0.8%)	6698 (1.1%)	13108 (2.1%)
Reservoirs						
humid tropics	23 (0.0%)	180 (0.0%)	1094 (0.2%)	3455 (0.6%)	7047 (1.1%)	6527 (1.1%)
wet-dry tropics	105 (0.0%)	1049 (0.2%)	3486 (0.6%)	8746 (1.4%)	22065 (3.6%)	15819 (2.6%)
(semi)arid (sub)tropics	85 (0.0%)	834 (0.1%)	2396 (0.4%)	4929 (0.8%)	10023 (1.6%)	13409 (2.2%)
humid subtropics	166 (0.0%)	2282 (0.4%)	5549 (0.9%)	11744 (1.9%)	14001 (2.3%)	7575 (1.2%)
highland (sub)tropics	28 (0.0%)	291 (0.0%)	855 (0.1%)	1673 (0.3%)	1874 (0.3%)	/

Table S14. Differences between GHG fluxes (mmol m^{-2} d^{-1}) from standing waterbodies across size classes. Values are shown as median (interquartile range; n=number of systems). Size classes in the first column are in km^2. P-values testing differences across size classes ('*p*-value size') are derived from Kruskal-Wallis tests, with post-hoc groupings indicated by letters based on pairwise Wilcoxon rank-sum tests with Benjamini-Hochberg correction ($p<0.05$). P-values testing differences between lakes and reservoirs within the same size class ('*p*-value type') were obtained using pairwise Kolmogorov-Smirnov tests. The table includes both measured and modelled fluxes based on measured concentrations (see Methods). P-values <0.05 are shown in bold and those <0.01 are shown in bold and italic.

	Reservoirs	**Lakes**	*p*-value 'type'
CO_2			
p-value 'size'	0.3539	0.1411	
<0.01	67.7 (39.0–120.8; n=15) (a)	53.8 (28.9–196.0; n=4) (a)	0.9203
0.01–0.1	41.9 (17.9–95.0; n=29) (a)	29.3 (14.4–50.7; n=7) (a)	0.5622
0.1–1	45.7 (7.5–97.4; n=27) (a)	7.8 (-5.0–74.9; n=27) (a)	0.1134
1–10	11.8 (0.7–89.1; n=30) (a)	5.3 (-5.5–26.2; n=22) (a)	0.1885
10–100	45.0 (15.0–176.6; n=42) (a)	13.4 (3.1–20.7; n=10) (a)	***0.0087***
100–1000	24.5 (6.8–118.2; n=21) (a)	7.6 (-9.3–29.8; n=13) (a)	**0.0492**
>1000	101.6 (26.6–227.7; n=5) (a)	1.5 (-2.7–22.8; n=12) (a)	**0.0269**
CH_4			
p-value 'size'	***0.0063***	0.4307	
<0.01	1.19 (0.27–7.64; n=22) (ab)	0.58 (0.12–7.21; n=18) (a)	0.3696
0.01–0.1	1.29 (0.41–5.31; n=32) (a)	0.35 (0.07–0.63; n=18) (a)	***0.0032***
0.1–1	0.37 (0.12–1.41; n=27) (ab)	0.34 (0.14–2.15; n=38) (a)	0.9363
1–10	0.36 (0.06–1.68; n=23) (ab)	0.25 (0.11–1.21; n=42) (a)	0.8370
10–100	0.38 (0.11–2.86; n=39) (ab)	0.37 (0.23–3.12; n=17) (a)	0.7552
100–1000	0.30 (0.05–0.87; n=25) (b)	0.61 (0.04–6.57; n=12) (a)	0.4753
>1000	2.10 (1.19–30.60; n=3) (ab)	0.18 (0.04–0.65; n=11) (a)	**0.0356**
N_2O			
p-value 'size'	0.2398	***0.0096***	
<0.01	0.015 (0.011–0.017; n=3) (a)	-0.002 (-0.002–-0.001; n=3) (a)	**0.0495**
0.01–0.1	0.059 (0.013–0.149; n=11) (a)	0.002 (-0.001–0.006; n=4) (abc)	**0.0188**
0.1–1	0.036 (0.007–0.057; n=8) (a)	-0.002 (-0.002–-0.001; n=16) (a)	***0.0040***
1–10	0.007 (0.004–0.013; n=3) (a)	-0.001 (-0.002–-0.000; n=11) (ab)	**0.0158**
10–100	0.012 (0.009–0.029; n=14) (a)	0.000 (0.000–0.000; n=1) (abc)	0.1649
100–1000	0.010 (0.009–0.025; n=11) (a)	0.000 (-0.001–0.035; n=5) (bc)	0.1262
>1000	0.400 (0.400–0.400; n=1) (a)	0.001 (0.001–0.002; n=6) (c)	0.1336

Table S15. Differences between GHG concentrations and k_{600} estimates (gas transfer velocity at Schmidt number 600) from standing waterbodies across size classes. Values are shown as median (interquartile range; n=number of systems). CO_2 and CH_4 values are in µM, N_2O values are in nM, and k_{600} estimates are in m d^{-1}. Size classes in the first column are in km^2. P-values testing differences across size classes ('*p*-value size') are derived from Kruskal-Wallis tests, with post-hoc groupings indicated by letters based on pairwise Wilcoxon rank-sum tests with Benjamini-Hochberg correction ($p<0.05$). P-values testing differences between lakes and reservoirs within the same size class ('*p*-value type') were obtained using pairwise Kolmogorov-Smirnov tests. P-values <0.05 are shown in bold and those <0.01 are shown in bold and italic.

	Reservoirs	**Lakes**	p-value 'type'
CO_2 (µM)			
p-value 'size'	0.9618	0.2295	
<0.01	59 (21–116; n=3) (a)	86 (48–294; n=4) (a)	0.4795
0.01–0.1	55 (45–94; n=12) (a)	50 (36–78; n=6) (a)	0.6396
0.1–1	46 (25–130; n=13) (a)	23 (4–148; n=22) (a)	0.2321
1–10	88 (30–142; n=19) (a)	14 (7–38; n=17) (a)	***0.0025***
10–100	55 (41–108; n=28) (a)	31 (26–33; n=6) (a)	**0.0239**
100–1000	73 (38–169; n=12) (a)	33 (16–51; n=10) (a)	**0.0296**
>1000	140 (29–254; n=4) (a)	24 (15–51; n=10) (a)	0.1573
CH_4 (µM)			
p-value 'size'	***3.46E-05***	**0.0279**	
<0.01	0.96 (0.42–1.61; n=7) (abc)	9.28 (0.39–46.70; n=5) (ab)	0.2912
0.01–0.1	2.00 (1.37–5.29; n=17) (a)	0.38 (0.08–226.99; n=9) (abc)	0.071
0.1–1	0.88 (0.26–1.86; n=18) (ab)	0.78 (0.17–21.53; n=28) (a)	0.5584
1–10	0.21 (0.10–0.69; n=13) (bc)	0.21 (0.09–0.58; n=30) (bc)	0.8531
10–100	0.13 (0.06–0.68; n=23) (bc)	0.25 (0.18–0.29; n=12) (abc)	0.3305
100–1000	0.08 (0.04–0.22; n=16) (c)	0.18 (0.05–0.53; n=9) (c)	0.4116
>1000	4.80 (0.30–9.30; n=2) (abc)	0.19 (0.05–0.30; n=9) (c)	0.099
N_2O (nM)			
p-value 'size'	***0.002***	***0.0058***	
<0.01	-	-	-
0.01–0.1	88.0 (27.5–106.2; n=9) (a)	7.5 (7.1–7.9; n=2) (ab)	**0.0339**
0.1–1	28.0 (17.4–46.5; n=7) (ab)	4.3 (1.9–6.8; n=11) (ab)	***9.42E-04***
1–10	14.0 (14.0–14.0; n=1) (ab)	1.9 (1.8–3.8; n=7) (a)	0.1221
10–100	9.1 (8.6–12.4; n=11) (b)	-	-
100–1000	10.1 (9.0–12.7; n=6) (b)	6.5 (5.4–78.6; n=5) (b)	0.4652
>1000	-	7.6 (7.1–8.2; n=6) (b)	-
k_{600} (m d^{-1})			
p-value 'size'	***2.22E-19***	***6.45E-06***	
<0.01	0.74 (0.68–0.76; n=23) (a)	1.02 (0.91–1.10; n=19) (a)	***7.27E-06***
0.01–0.1	0.77 (0.75–0.93; n=35) (b)	1.12 (0.93–1.21; n=20) (abc)	***2.12E-05***
0.1–1	0.96 (0.85–1.04; n=31) (c)	1.00 (0.94–1.23; n=45) (ab)	**0.0441**
1–10	1.06 (0.98–1.24; n=37) (de)	1.13 (1.04–1.23; n=46) (bc)	0.2921
10–100	1.07 (0.95–1.15; n=54) (d)	1.20 (1.12–1.26; n=19) (c)	**0.0119**
100–1000	1.15 (1.05–1.27; n=30) (e)	1.28 (1.22–1.39; n=14) (d)	0.0555
>1000	1.14 (0.98–1.46; n=5) (cde)	1.33 (1.21–1.44; n=12) (d)	0.3991

Table S16a. Differences between GHG fluxes (mmol m^{-2} d^{-1}) from standing waterbodies across climate zones. Values are shown as median (interquartile range; n=number of systems). P-values are derived from Kruskal-Wallis tests, and post-hoc groupings based on pairwise Wilcoxon rank-sum tests with Benjamini-Hochberg correction are indicated by letters; climate zones sharing the same letter are not significantly different ($p<0.05$). Flux values include both measured and modelled estimates. P-values <0.05 are shown in bold and those <0.01 are shown in bold and italic.

	CO_2	CH_4	N_2O
***p*-value**	**0.0388**	0.1335	***2.16E-07***
humid	91.3 (15.0–240.9; n=18) (a)	1.06 (0.26–9.59; n=30) (a)	0.009 (0.004–0.041; n=13) (a)
wet-dry	7.8 (-2.8–70.9; n=65) (b)	0.56 (0.12–3.29; n=70) (a)	-0.000 (-0.002–0.009; n=32) (b)
arid	10.5 (9.0–78.4; n=7) (a)	0.19 (0.06–9.71; n=9) (a)	0.012 (0.009–0.021; n=4) (a)
humid sub.	31.9 (5.4–89.1; n=146) (a)	0.45 (0.13–1.51; n=148) (a)	0.025 (0.009–0.068; n=30) (a)
highland	21.6 (9.6–63.9; n=27) (a)	0.30 (0.11–1.27; n=76) (a)	-0.001 (-0.002–-0.000; n=17) (b)

Table S16b. Differences between GHG concentrations and k_{600} estimates (gas transfer velocity at Schmidt number 600) from standing waterbodies across climate zones. Values are shown as median (interquartile range; n=number of systems). P-values are derived from Kruskal-Wallis tests, and post-hoc groupings based on pairwise Wilcoxon rank-sum tests with Benjamini-Hochberg correction are indicated by letters; climate zones sharing the same letter are not significantly different ($p<0.05$). P-values <0.05 are shown in bold and those <0.01 are shown in bold and italic.

	CO_2 (µM)	CH_4 (µM)	N_2O (nM)	k_{600} (m d^{-1})
***p*-value**	0.2662	0.801	***5.34E-08***	***5.83E-04***
humid	63 (28–152; n=14) (a)	0.30 (0.10–1.04; n=21) (a)	10.7 (7.9–15.4; n=8) (a)	1.03 (0.84–1.19; n=32) (a)
wet-dry	21 (12–130; n=38) (a)	0.46 (0.09–2.04; n=56) (a)	5.2 (2.2–8.1; n=28) (b)	1.02 (0.94–1.20; n=78) (a)
arid	55 (34–127; n=6) (a)	0.28 (0.09–1.30; n=7) (a)	12.6 (9.3–21.9; n=4) (ac)	1.03 (0.94–1.16; n=12) (ab)
humid sub.	46 (28–94; n=86) (a)	0.26 (0.11–1.12; n=61) (a)	28.0 (13.3–92.8; n=21) (c)	1.01 (0.85–1.20; n=192) (a)
highland	56 (34–118; n=21) (a)	0.25 (0.10–1.89; n=52) (a)	7.5 (7.2–7.8; n=3) (ab)	1.14 (1.04–1.24; n=74) (b)

Table S17. Differences between ebullitive CH_4 fluxes (mmol m^{-2} d^{-1}) from standing waterbodies across climate zones. Values are shown as median (interquartile range; n=number of observations). The p-value is derived from a Kruskal-Wallis test, and post-hoc groupings based on pairwise Wilcoxon rank-sum tests with Benjamini-Hochberg correction are indicated by letters; climate zones sharing the same letter are not significantly different ($p<0.05$).

Climate zone	ebullitive CH_4 flux
***p*-value**	***4.5808e-07***
humid	0.39 (0.00–6.48, n=114) (a)
wet-dry	9.65 (5.50–19.24, n=12) (b)
arid	0.13 (0.02–12.88, n=8) (ab)
humid sub.	7.24 (0.48–24.42, n=101) (b)
highland	2.11 (0.38–23.62, n=31) (ab)
TOTAL	**2.01 (0.04–14.64, n=286)**

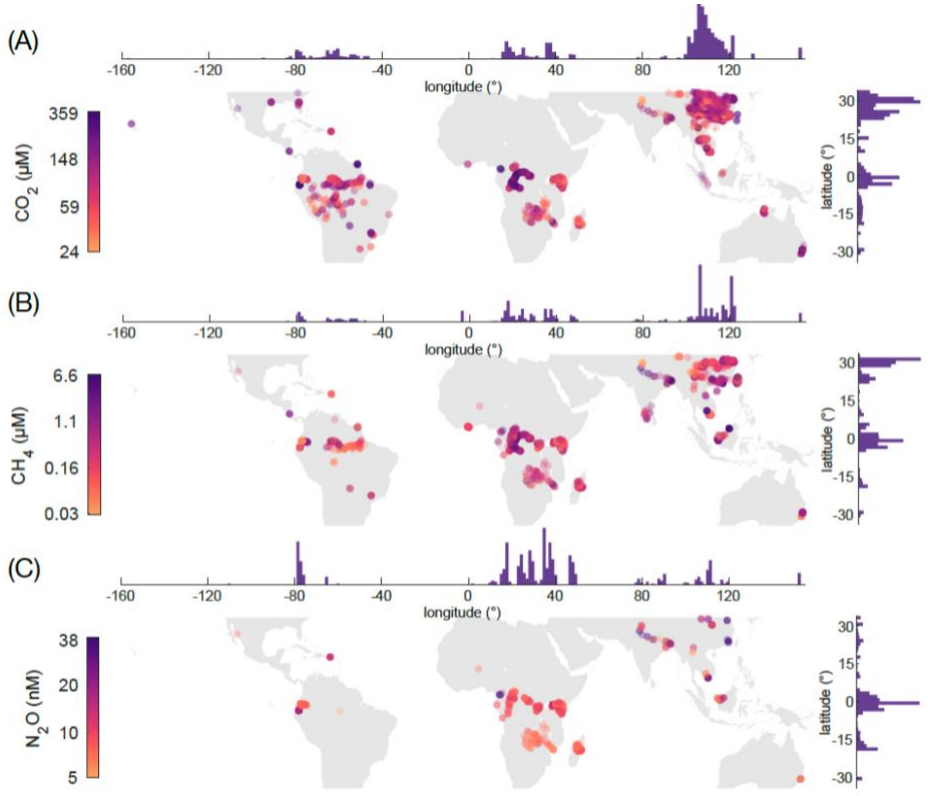

Figure S4. Spatial distribution of median GHG concentrations in streams and rivers of the (sub)tropics.

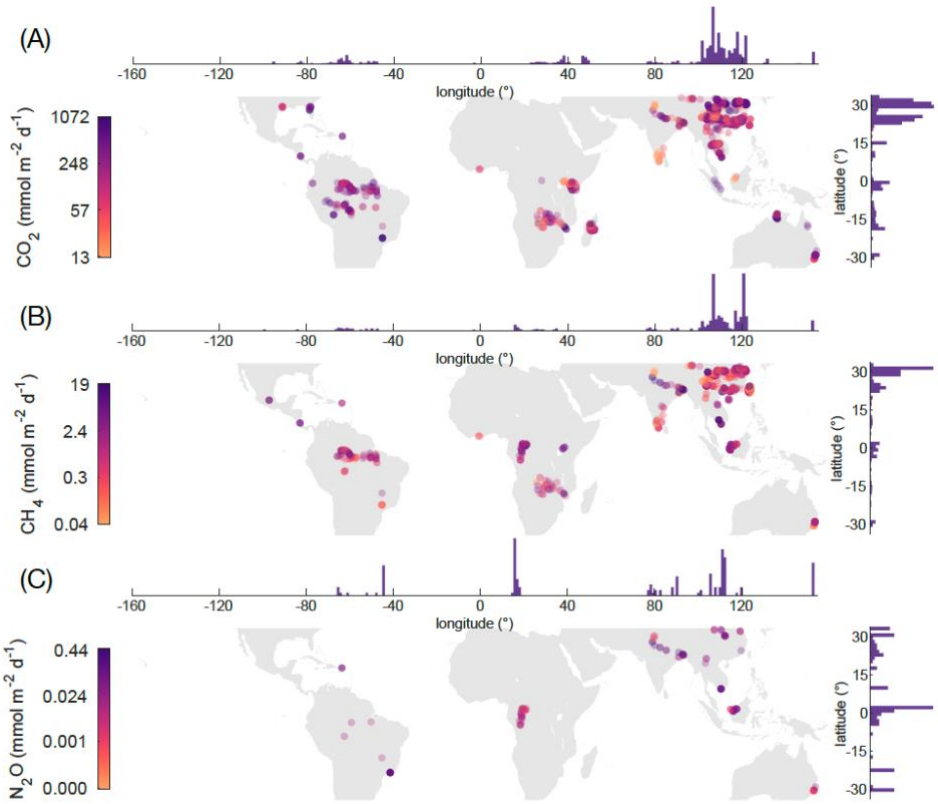

Figure S5. Spatial distribution of median GHG fluxes in streams and rivers of the (sub)tropics. CH_4 fluxes only include diffusive flux estimates. Fluxes estimated based on concentration measurements and gas transfer velocity estimates are not included.

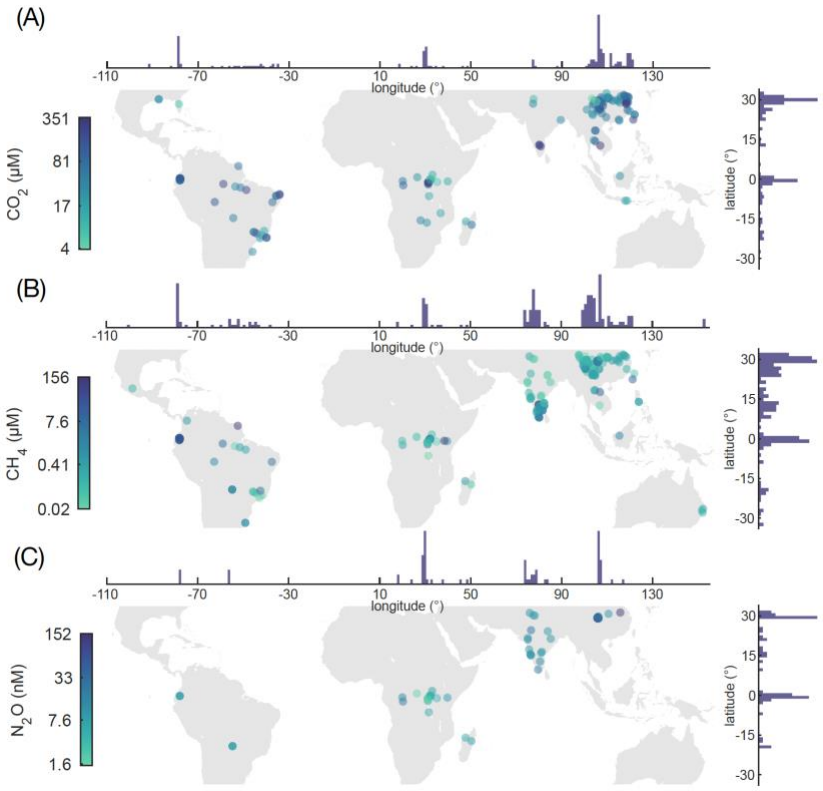

Figure S6. Spatial distribution of median GHG concentrations in lakes and reservoirs of the (sub)tropics. Each marker corresponds to one lake/reservoir.

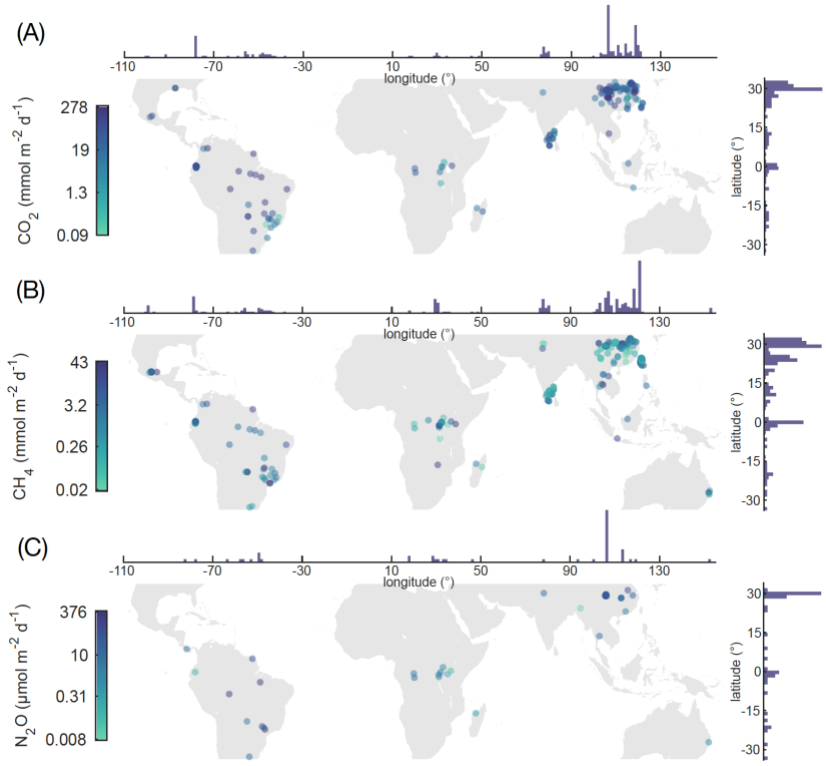

Figure S7. Spatial distribution of median GHG fluxes in lakes and reservoirs of the (sub)tropics. CH_4 fluxes only include diffusive flux estimates. Fluxes estimated based on concentration measurements and gas transfer velocity estimates are not included. Each marker corresponds to one lake/reservoir.

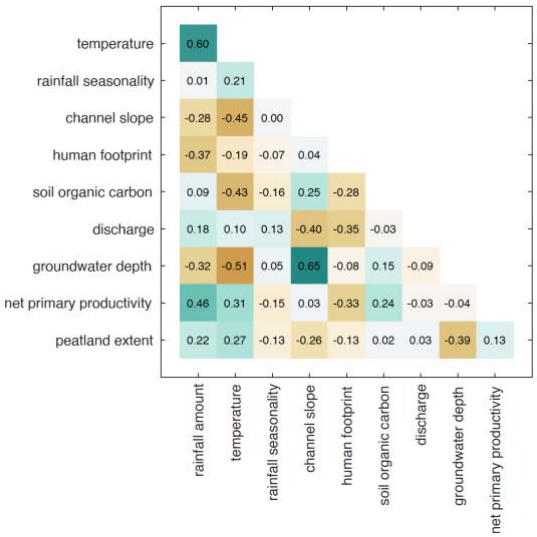

Figure S8. Correlation matrix showing pairwise Spearman correlation coefficients among predictor variables retained in the random forest models. Strong positive correlations are indicated in dark green and strong negative correlations in dark brown.

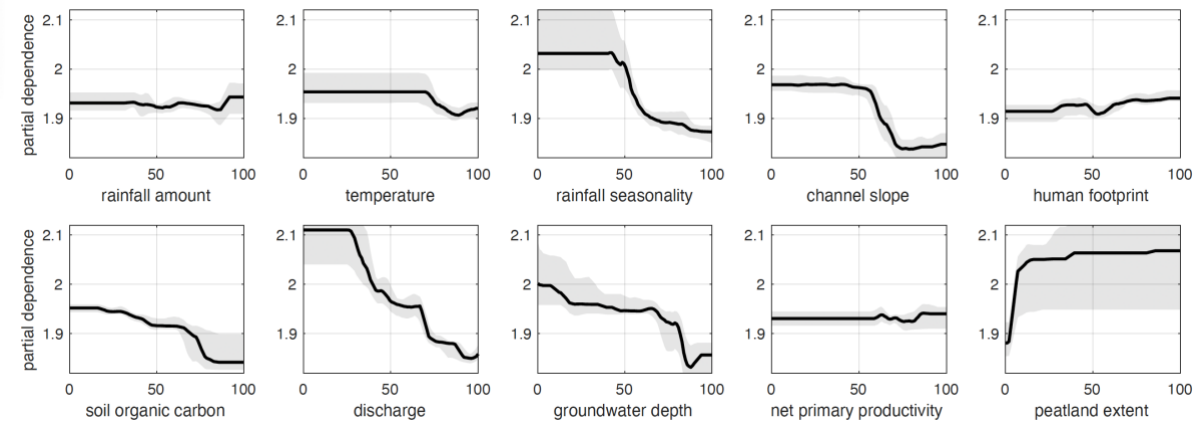

Figure S9. Partial dependence plots for riverine CO_2 concentrations based on best random forest model. Predictors are scaled to 0-100 for comparison across variables.

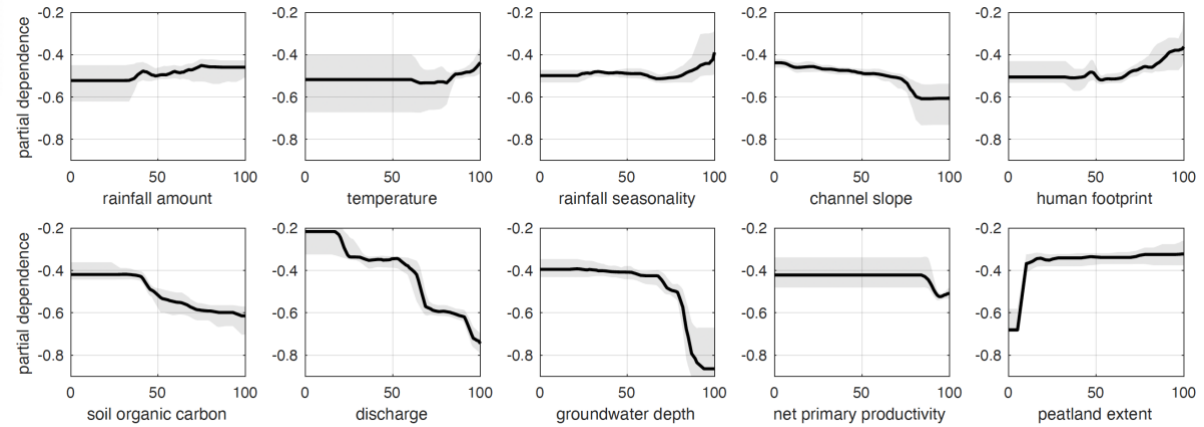

Figure S10. Partial dependence plots for CH_4 concentrations based on best random forest model. Predictors are scaled to 0-100 for comparison across variables.

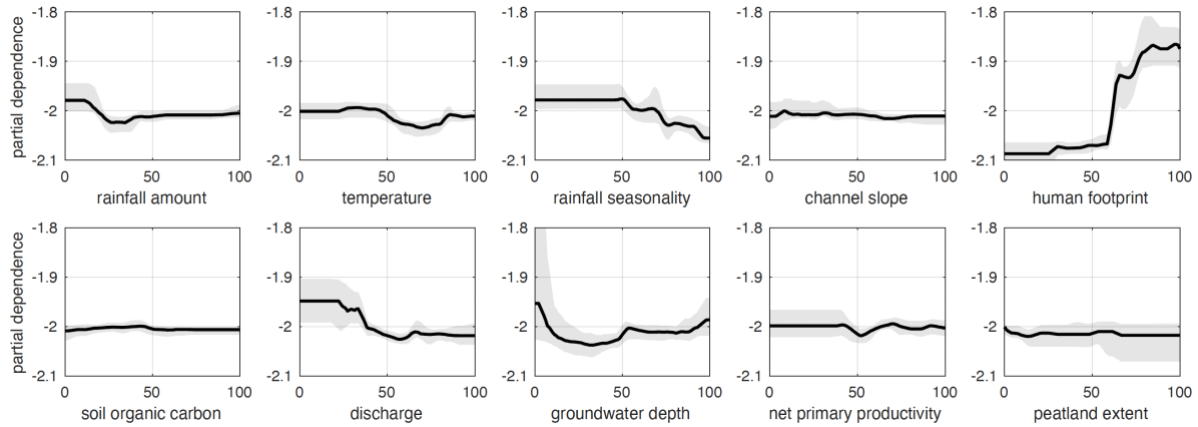

Figure S11. Partial dependence plots for N_2O concentrations based on best random forest model. Predictors are scaled to 0-100 for comparison across variables.

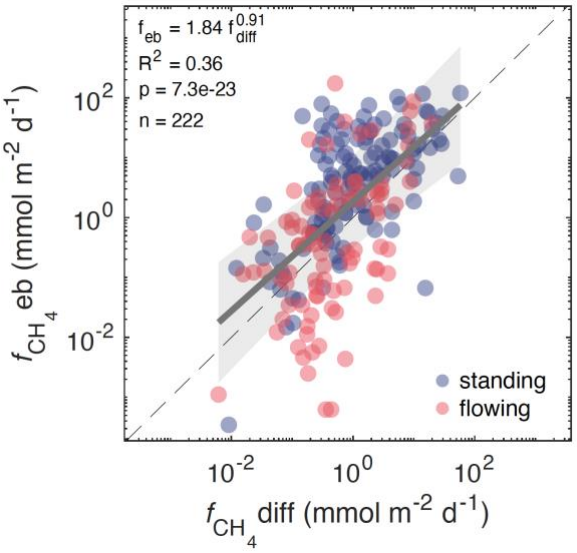

Figure S12. Power-law regression fitted to the diffusive ($f_{CH4\ diff}$) and ebullitive ($f_{CH4\ eb}$) fluxes measured in both flowing and standing waters. The thick grey line represents the power-law regression while the light grey shaded area represents the 95% confidence intervals. The dashed line in the background denotes the 1:1 line. Sites or systems with several observations were averaged out.

References

1 Lorke, A. *et al.* Technical note: drifting versus anchored flux chambers for measuring greenhouse gas emissions from running waters. *Biogeosciences* **12**, 7013-7024, doi:10.5194/bg-12-7013-2015 (2015).
2 Rexroade, A. T., Wallin, M. B. & Duvert, C. Measuring gas transfer velocity in a steep tropical stream: Method evaluation and implications for upscaling. *Journal of Geophysical Research: Biogeosciences* **130**, e2024JG008420, doi:10.1029/2024JG008420 (2025).
3 Gómez-Gener, L. *et al.* Global carbon dioxide efflux from rivers enhanced by high nocturnal emissions. *Nature Geoscience* **14**, 289-294, doi:10.1038/s41561-021-00722-3 (2021).
4 Woodrow, R. L. *et al.* Enhanced stream greenhouse gas emissions at night and during flood events. *Limnology and Oceanography Letters* **9**, 276-285, doi:10.1002/lol2.10374 (2024).
5 Rudberg, D. *et al.* Diel variability of CO2 emissions from northern lakes. *Journal of Geophysical Research: Biogeosciences* **126**, e2021JG006246, doi:10.1029/2021JG006246 (2021).
6 Sieczko, A. K. *et al.* Diel variability of methane emissions from lakes. *Proceedings of the National Academy of Sciences* **117**, 21488-21494, doi:10.1073/pnas.2006024117 (2020).
7 Borges, A. V. *et al.* Variations in dissolved greenhouse gases (CO2, CH4, N2O) in the Congo River network overwhelmingly driven by fluvial-wetland connectivity. *Biogeosciences* **16**, 3801-3834, doi:10.5194/bg-16-3801-2019 (2019).
8 Borges, A. V. *et al.* Greenhouse gas emissions from African lakes are no longer a blind spot. *Science Advances* **8**, eabi8716, doi:10.1126/sciadv.abi8716 (2022).
9 Bauduin, T., Gypens, N. & Borges, A. V. Sub-daily variability of carbon dioxide, methane, and nitrous oxide emissions from two urban ponds in Brussels (Belgium). *Journal of Environmental Management* **373**, 123627, doi:10.1016/j.jenvman.2024.123627 (2025).
10 Melack, J. M. Temporal variability of phytoplankton in tropical lakes. *Oecologia* **44**, 1-7, doi:10.1007/BF00346388 (1979).
11 Liu, S. *et al.* The importance of hydrology in routing terrestrial carbon to the atmosphere via global streams and rivers. *Proceedings of the National Academy of Sciences* **119**, e2106322119, doi:10.1073/pnas.2106322119 (2022).
12 Rocher-Ros, G. *et al.* Global methane emissions from rivers and streams. *Nature* **621**, 530-535, doi:10.1038/s41586-023-06344-6 (2023).
13 Crawford, J. T., Dornblaser, M. M., Stanley, E. H., Clow, D. W. & Striegl, R. G. Source limitation of carbon gas emissions in high-elevation mountain streams and lakes. *Journal of Geophysical Research: Biogeosciences* **120**, 952-964, doi:10.1002/2014JG002861 (2015).
14 Rocher-Ros, G., Sponseller, R. A., Lidberg, W., Mörth, C.-M. & Giesler, R. Landscape process domains drive patterns of CO2 evasion from river networks. *Limnology and Oceanography Letters* **4**, 87-95, doi:10.1002/lol2.10108 (2019).
15 Solano, V. *et al.* Stream respiration exceeds CO2 evasion in a low-energy, oligotrophic tropical stream. *Limnology and Oceanography* **68**, 1132-1146, doi:10.1002/lno.12334 (2023).
16 Richey, J. E., Melack, J. M., Aufdenkampe, A. K., Ballester, V. M. & Hess, L. L. Outgassing from Amazonian rivers and wetlands as a large tropical source of atmospheric CO2. *Nature* **416**, 617-620, doi:10.1038/416617a (2002).
17 Bouillon, S. *et al.* Contrasting biogeochemical characteristics of the Oubangui River and tributaries (Congo River basin). *Scientific Reports* **4**, 5402, doi:10.1038/srep05402 (2014).
18 Saccardi, B. & Winnick, M. Improving predictions of stream CO2 concentrations and fluxes using a stream network model: A case study in the East River Watershed, CO, USA. *Global Biogeochemical Cycles* **35**, e2021GB006972, doi:10.1029/2021GB006972 (2021).
19 Tian, H. *et al.* Increased terrestrial carbon export and CO2 evasion from global inland waters since the Preindustrial Era. *Global Biogeochemical Cycles* **37**, e2023GB007776, doi:10.1029/2023GB007776 (2023).
20 Saccardi, B., Brinkerhoff, C. B., Gleason, C. J. & Winnick, M. J. Toward modeling continental-scale inland water carbon dioxide emissions. *AGU Advances* **5**, e2024AV001294, doi:10.1029/2024AV001294 (2024).
21 Morana, C. *et al.* Prevalence of autotrophy in non-humic African lakes. *Ecosystems* **26**, 627-642, doi:10.1007/s10021-022-00783-4 (2023).
22 Rosentreter, J. A. *et al.* Half of global methane emissions come from highly variable aquatic ecosystem sources. *Nature Geoscience* **14**, 225-230, doi:10.1038/s41561-021-00715-2 (2021).
23 Johnson, M. S., Matthews, E., Du, J., Genovese, V. & Bastviken, D. Methane emission from global lakes: New spatiotemporal data and observation-driven modeling of methane dynamics indicates lower emissions. *Journal of Geophysical Research: Biogeosciences* **127**, e2022JG006793, doi:10.1029/2022JG006793 (2022).
24 Vachon, D., Prairie, Y. T. & Cole, J. J. The relationship between near-surface turbulence and gas transfer velocity in freshwater systems and its implications for floating chamber measurements of gas exchange. *Limnology and Oceanography* **55**, 1723-1732, doi:10.4319/lo.2010.55.4.1723 (2010).
25 Vingiani, F. *et al.* Evaluating stream CO2 outgassing via drifting and anchored flux chambers in a controlled flume experiment. *Biogeosciences* **18**, 1223-1240, doi:10.5194/bg-18-1223-2021 (2021).
26 Ulseth, A. J. *et al.* Distinct air–water gas exchange regimes in low- and high-energy streams. *Nature Geoscience* **12**, 259-263, doi:10.1038/s41561-019-0324-8 (2019).
27 Raymond, P. A. *et al.* Scaling the gas transfer velocity and hydraulic geometry in streams and small rivers. *Limnology and Oceanography: Fluids and Environments* **2**, 41-53, doi:10.1215/21573689-1597669 (2012).
28 Klaus, M. & Vachon, D. Challenges of predicting gas transfer velocity from wind measurements over global lakes. *Aquatic Sciences* **82**, 53, doi:10.1007/s00027-020-00729-9 (2020).
29 Wanninkhof, R. Relationship between wind speed and gas exchange over the ocean. *Journal of Geophysical Research: Oceans* **97**, 7373-7382, doi:10.1029/92JC00188 (1992).

30 Vachon, D. & Prairie, Y. T. The ecosystem size and shape dependence of gas transfer velocity versus wind speed relationships in lakes. *Canadian Journal of Fisheries and Aquatic Sciences* **70**, 1757-1764, doi:10.1139/cjfas-2013-0241 (2013).
31 Cole, J. J. & Caraco, N. F. Atmospheric exchange of carbon dioxide in a low-wind oligotrophic lake measured by the addition of SF6. *Limnology and Oceanography* **43**, 647-656, doi:10.4319/lo.1998.43.4.0647 (1998).
32 Fick, S. E. & Hijmans, R. J. WorldClim 2: new 1-km spatial resolution climate surfaces for global land areas. *International Journal of Climatology* **37**, 4302-4315, doi:10.1002/joc.5086 (2017).
33 Amatulli, G. *et al.* Hydrography90m: a new high-resolution global hydrographic dataset. *Earth System Science Data* **14**, 4525-4550, doi:10.5194/essd-14-4525-2022 (2022).
34 Wallin, M. B. *et al.* Carbon dioxide and methane emissions of Swedish low-order streams—a national estimate and lessons learnt from more than a decade of observations. *Limnology and Oceanography Letters* **3**, 156-167, doi:10.1002/lol2.10061 (2018).
35 Leopold, L. B. & Maddock, T. J. The hydraulic geometry of stream channels and some physiographic implications. Report No. 252, 64 (Washington, D.C., 1953).
36 DelSontro, T., McGinnis, D. F., Wehrli, B. & Ostrovsky, I. Size does matter: Importance of large bubbles and small-scale hot spots for methane transport. *Environmental Science & Technology* **49**, 1268-1276, doi:10.1021/es5054286 (2015).
37 Linkhorst, A. *et al.* Comparing methane ebullition variability across space and time in a Brazilian reservoir. *Limnology and Oceanography* **65**, 1623-1634, doi:10.1002/lno.11410 (2020).
38 Wilkinson, J., Bodmer, P. & Lorke, A. Methane dynamics and thermal response in impoundments of the Rhine River, Germany. *Science of The Total Environment* **659**, 1045-1057, doi:10.1016/j.scitotenv.2018.12.424 (2019).
39 Vähä, A. *et al.* Temporal dynamics and environmental controls of carbon dioxide and methane fluxes measured by the eddy covariance method over a boreal river. *EGUsphere* **2024**, 1-30, doi:10.5194/egusphere-2024-1644 (2024).
40 Sawakuchi, H. O. *et al.* Methane emissions from Amazonian Rivers and their contribution to the global methane budget. *Global Change Biology* **20**, 2829-2840, doi:10.1111/gcb.12646 (2014).
41 Zhang, L. *et al.* Significant methane ebullition from alpine permafrost rivers on the East Qinghai–Tibet Plateau. *Nature Geoscience* **13**, 349-354, doi:10.1038/s41561-020-0571-8 (2020).
42 Crawford, J. T. *et al.* Ebullitive methane emissions from oxygenated wetland streams. *Global Change Biology* **20**, 3408-3422, doi:10.1111/gcb.12614 (2014).
43 Baulch, H. M., Dillon, P. J., Maranger, R. & Schiff, S. L. Diffusive and ebullitive transport of methane and nitrous oxide from streams: Are bubble-mediated fluxes important? *Journal of Geophysical Research: Biogeosciences* **116**, doi:10.1029/2011JG001656 (2011).
44 Wilcock, R. J. & Sorrell, B. K. Emissions of Greenhouse Gases CH4 and N2O from Low-gradient Streams in Agriculturally Developed Catchments. *Water, Air, and Soil Pollution* **188**, 155-170, doi:10.1007/s11270-007-9532-8 (2008).
45 Spawn, S. A. *et al.* Summer methane ebullition from a headwater catchment in Northeastern Siberia. *Inland Waters* **5**, 224-230, doi:10.5268/IW-5.3.845 (2015).
46 Maeck, A., Hofmann, H. & Lorke, A. Pumping methane out of aquatic sediments — ebullition forcing mechanisms in an impounded river. *Biogeosciences* **11**, 2925-2938, doi:10.5194/bg-11-2925-2014 (2014).
47 McGinnis, D. F. *et al.* Deconstructing Methane Emissions from a Small Northern European River: Hydrodynamics and Temperature as Key Drivers. *Environmental Science & Technology* **50**, 11680-11687, doi:10.1021/acs.est.6b03268 (2016).
48 Wilkinson, J., Maeck, A., Alshboul, Z. & Lorke, A. Continuous Seasonal River Ebullition Measurements Linked to Sediment Methane Formation. *Environmental Science & Technology* **49**, 13121-13129, doi:10.1021/acs.est.5b01525 (2015).
49 Robison, A. L. *et al.* Spatial and temporal heterogeneity of methane ebullition in lowland headwater streams and the impact on sampling design. *Limnology and Oceanography* **66**, 4063-4076, doi:10.1002/lno.11943 (2021).
50 Bednařík, A., Bodmer, P., Darenova, E., Kokrda, L. & Pavelka, M. Temperature, Water Depth, and Flow Velocity Are Important Drivers of Methane Ebullition in a Temperate Lowland Stream. *Journal of Geophysical Research: Biogeosciences* **129**, e2023JG007597, doi:10.1029/2023JG007597 (2024).
51 Bednarik A *et al.* Chasing bubbles: towards a standardized approach for quantifying methane ebullition in streams and rivers. *Zenodo*, doi:10.5281/zenodo.15696475 (2025).
52 Maeck, A. *et al.* Sediment Trapping by Dams Creates Methane Emission Hot Spots. *Environmental Science & Technology* **47**, 8130-8137, doi:10.1021/es4003907 (2013).
53 Holgerson, M. A. & Raymond, P. A. Large contribution to inland water CO2 and CH4 emissions from very small ponds. *Nature Geoscience* **9**, 222-226, doi:10.1038/ngeo2654 (2016).
54 Downing, J. A. *et al.* The global abundance and size distribution of lakes, ponds, and impoundments. *Limnology and Oceanography* **51**, 2388-2397, doi:10.4319/lo.2006.51.5.2388 (2006).
55 Seekell, D. A. & Pace, M. L. Does the Pareto distribution adequately describe the size-distribution of lakes? *Limnology and Oceanography* **56**, 350-356, doi:10.4319/lo.2011.56.1.0350 (2011).
56 Verpoorter, C., Kutser, T., Seekell, D. A. & Tranvik, L. J. A global inventory of lakes based on high-resolution satellite imagery. *Geophysical Research Letters* **41**, 6396-6402, doi:10.1002/2014GL060641 (2014).
57 McDonald, C. P., Rover, J. A., Stets, E. G. & Striegl, R. G. The regional abundance and size distribution of lakes and reservoirs in the United States and implications for estimates of global lake extent. *Limnology and Oceanography* **57**, 597-606, doi:10.4319/lo.2012.57.2.0597 (2012).
58 Wang, J. *et al.* The Surface Water and Ocean Topography Mission (SWOT) Prior Lake Database (PLD): Lake Mask and Operational Auxiliaries. *Water Resources Research* **61**, e2023WR036896, doi:10.1029/2023WR036896 (2025).

59 Seekell, D. A., Pace, M. L., Tranvik, L. J. & Verpoorter, C. A fractal-based approach to lake size-distributions. *Geophysical Research Letters* **40**, 517-521, doi:10.1002/grl.50139 (2013).
60 Messager, M. L., Lehner, B., Grill, G., Nedeva, I. & Schmitt, O. Estimating the volume and age of water stored in global lakes using a geo-statistical approach. *Nature Communications* **7**, 13603, doi:10.1038/ncomms13603 (2016).
61 Lin, P. *et al.* Global reconstruction of naturalized river flows at 2.94 million reaches. *Water Resources Research* **55**, 6499-6516, doi:10.1029/2019WR025287 (2019).
62 Huttunen, J. T. *et al.* Fluxes of methane, carbon dioxide and nitrous oxide in boreal lakes and potential anthropogenic effects on the aquatic greenhouse gas emissions. *Chemosphere* **52**, 609-621, doi:10.1016/S0045-6535(03)00243-1 (2003).
63 Hyvönen, T., Ojala, A., Kankaala, P. & Martikainen, P. J. Methane release from stands of water horsetail (Equisetum fluviatile) in a boreal lake. *Freshwater Biology* **40**, 275-284, doi:10.1046/j.1365-2427.1998.00351.x (1998).
64 Juutinen, S. *et al.* Major implication of the littoral zone for methane release from boreal lakes. *Global Biogeochemical Cycles* **17**, doi:10.1029/2003GB002105 (2003).
65 Desrosiers, K., DelSontro, T. & del Giorgio, P. A. Disproportionate contribution of vegetated habitats to the CH4 and CO2 budgets of a boreal lake. *Ecosystems* **25**, 1522-1541, doi:10.1007/s10021-021-00730-9 (2022).
66 Grasset, C., Mesman, J. P., Tranvik, L. J., Maranger, R. & Sobek, S. Contribution of lake littoral zones to the continental carbon budget. *Nature Geoscience* **18**, 747-752, doi:10.1038/s41561-025-01739-8 (2025).
67 Hammer, U. T. & Heseltine, J. M. Aquatic macrophytes in saline lakes of the Canadian prairies. *Hydrobiologia* **158**, 101-116, doi:10.1007/BF00026269 (1988).
68 Bayley, S. E. & Prather, C. M. Do wetland lakes exhibit alternative stable states? Submersed aquatic vegetation and chlorophyll in western boreal shallow lakes. *Limnology and Oceanography* **48**, 2335-2345, doi:10.4319/lo.2003.48.6.2335 (2003).
69 Bartlett, K. B. *et al.* Methane flux from the central Amazonian floodplain. *Journal of Geophysical Research: Atmospheres* **93**, 1571-1582, doi:10.1029/JD093iD02p01571 (1988).
70 Devol, A. H., Richey, J. E., Clark, W. A., King, S. L. & Martinelli, L. A. Methane emissions to the troposphere from the Amazon floodplain. *Journal of Geophysical Research: Atmospheres* **93**, 1583-1592, doi:10.1029/JD093iD02p01583 (1988).
71 Melack, J. M. *et al.* Regionalization of methane emissions in the Amazon Basin with microwave remote sensing. *Global Change Biology* **10**, 530-544, doi:10.1111/j.1365-2486.2004.00763.x (2004).
72 Abril, G. *et al.* Amazon River carbon dioxide outgassing fuelled by wetlands. *Nature* **505**, 395-398, doi:10.1038/nature12797 (2014).
73 Pangala, S. R. *et al.* Large emissions from floodplain trees close the Amazon methane budget. *Nature* **552**, 230-234, doi:10.1038/nature24639 (2017).
74 Borges, A. V. *et al.* Globally significant greenhouse-gas emissions from African inland waters. *Nature Geoscience* **8**, 637-642, doi:10.1038/ngeo2486 (2015).
75 Zhang, Z. *et al.* Emerging role of wetland methane emissions in driving 21st century climate change. *Proceedings of the National Academy of Sciences* **114**, 9647-9652, doi:10.1073/pnas.1618765114 (2017).
76 Peng, S. *et al.* Wetland emission and atmospheric sink changes explain methane growth in 2020. *Nature* **612**, 477-482, doi:10.1038/s41586-022-05447-w (2022).
77 Zhang, Z. *et al.* Recent intensification of wetland methane feedback. *Nature Climate Change* **13**, 430-433, doi:10.1038/s41558-023-01629-0 (2023).
78 Zhu, Q. *et al.* Advancements and opportunities to improve bottom–up estimates of global wetland methane emissions. *Environmental Research Letters* **20**, 023001, doi:10.1088/1748-9326/adad02 (2025).
79 Melack, J. M. *et al.* Challenges regionalizing methane emissions using aquatic environments in the Amazon Basin as examples. *Frontiers in Environmental Science* **10**, doi:10.3389/fenvs.2022.866082 (2022).
80 Lehner, B. *et al.* Mapping the world's inland surface waters: an upgrade to the Global Lakes and Wetlands Database (GLWD v2). *Earth System Science Data* **17**, 2277-2329, doi:10.5194/essd-17-2277-2025 (2025).
81 Jeffrey, L. C. *et al.* Large methane emissions from tree stems complicate the wetland methane budget. *Journal of Geophysical Research: Biogeosciences* **128**, e2023JG007679, doi:10.1029/2023JG007679 (2023).
82 Fluet-Chouinard, E. *et al.* Extensive global wetland loss over the past three centuries. *Nature* **614**, 281-286, doi:10.1038/s41586-022-05572-6 (2023).
83 Hübinger, C., Fluet-Chouinard, E., Hugelius, G., Peña, F. J. & Jaramillo, F. Automating the detection of hydrological barriers and fragmentation in wetlands using deep learning and InSAR. *Remote Sensing of Environment* **311**, 114314, doi:10.1016/j.rse.2024.114314 (2024).